RAM. ROBOTICS AND MECHATRONICS

TOWARDS CONTROL OF SOFT ROBOTIC KNEE BRACE FOR ACL DEFICIENT PATIENTS

M. (Mitul) Agrawal

MSC ASSIGNMENT

Committee:
dr. ir. J.F. Broenink
dr. H. Naghibi Beidokhti
dr. ir. M. Abayazid
dr. ir. M. Vlutters

February, 2021

004RaM2021
Robotics and Mechatronics
EEMCS
University of Twente
P.O. Box 217
7500 AE Enschede
The Netherlands

UNIVERSITY OF TWENTE. | TECHMED CENTRE UNIVERSITY OF TWENTE. | DIGITAL SOCIETY INSTITUTE

Abstract

Anterior Cruciate Ligament (ACL) is one of the ligaments in the knee joint responsible for its stability during motion. This ligament is most prone to partial or complete tear during any contact or non-contact injury related to the knee. The injury causes stability issues in the knee while performing daily living activities making reconstruction surgery a common choice. Surgery requires replacement of ligament with nearby muscle fibers from hamstring or quadriceps muscle groups. Surgery can be avoided in some cases but requires costly rehabilitative trials to strengthen hamstring muscle activation to provide stability to a knee with ACL deficiency. Recently a commercial knee brace was equipped with Pneumatic Artificial Muscles (PAM) which revealed effectiveness in reducing hamstring activation. PAMs are compliant high-density actuators suitable for usage as an actuation system in the knee brace to assist human muscles.

Past studies have shown the effect of PAM actuated brace on hamstring muscle activation. However, a deeper understanding is required to understand the influence of PAM actuation on hamstring activations in order to control the knee brace actuation system. To achieve this understanding without invasive techniques on patients, a Neuro Musculoskeletal Model (NMM) is needed. Such models help in understanding the interactions between the neural signals and muscles which dictate the muscle dynamics. Muscle dynamics when combined with the skeletal model of the human body allows the simulation of all the muscles working in tandem with each other to produce realistic motion and internal properties.

In this study using NMMs, different aspects of the actuation mechanism (using PAMs) on hamstring muscle activities are studied and presented. A NMM for the lower extremity is run using Opensim software for forward simulations with the PAM actuated brace attached to the knee joint. The study focuses on PAM actuated braces' capacity to compliment hamstring muscles during self-paced walking. Hamstring facilitation is a strategy to help stabilize the knee during the rehabilitation of patients with ACL deficiency and patients after ACL reconstruction surgery.

Contents

List of Abbreviations

ACL Anterior Cruciate Ligament

ATT Anterior Tibial Translation

BFLH Biceps Femoris Long Head

BFSH Biceps Femoris Short Head

CMC Computed Muscle Control

CT X-Ray Computed Tomography

DoF Degrees of Freedom

IMU Inertial Measurement Unit

MRI Magnetic Resonance Imaging

NMM Neuro Musculoskeletal Model

PAM Pneumatic Artificial Muscle

sEMG surface ElectroMyoGraph

SM SemiMembranosus

ST SemiTendonous

1 Introduction

The knee joint is a complex joint in the human body responsible for bearing the most of body load during any activity being performed by the human body. It comprises multiple structures, including bones, muscles, ligaments, meniscus, and the patella as shown in Fig. 1.1. Anterior Cruciate Ligament (ACL) is a ligament in our knee joining the bottom back of our thigh bone (femur) with the front top of our shinbone (tibia), providing us stability during walking, sprinting, squatting, etc. Tear to this ligament causes loss of knee restrictions (constraints), allowing larger translations between femur and tibia, known as Anterior Tibial Translation (ATT). ATT value ranges from 3-6 mm for normal patients, while for ACL-deficient (ACLd) patients it reaches 7-15 mm translation. ACL rupture is a common injury in sports, which happens due to the strain to ACL during impact, sudden motion, and/or twisting of the knee (to change direction), causing it to tear, making the knee ACLd. This injury can happen in daily life even without a fall or impact, making it an overall common knee injury. Such long term ailments can cause osteoarthritis, which finally leads to knee replacement.

Knee braces are generally used to prevent ACL injuries in strenuous sports training or skiing boots. ACL-reconstruction (ACLr) surgery is the most chosen option for athletes aiming to return to their sports again after an injury. Knee braces are provided to patients who are about to undergo surgery. Knee braces are widely used post-surgery or/and post-injury for providing support during rehabilitation. During rehabilitation with such braces, it has been seen that it does not provide any benefit to ATT due to ACLd knee in weight-bearing activities (Beynnon et al., 2003).

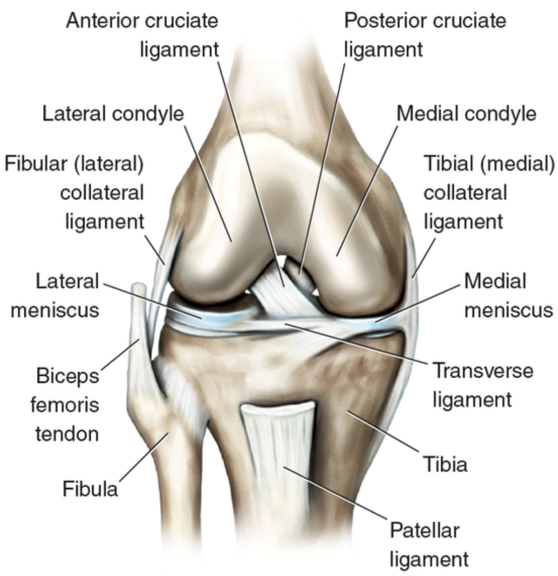

Figure 1.1: Lateral view of anatomy of right leg knee. (Physiopedia, 2016)

Hamstrings and quadriceps muscles are responsible for knee flexion. Hamstrings are a crucial group of muscles responsible for ATT and knee stability. It is attached to the femurs posterior (backward) side, which ends at the hip and the tibia bones. The hamstrings provide the force needed to flex the knee. They also pull the tibia posteriorly relative to the femur, acting as a dynamic protector of the ACL and reducing strain on the ligament.

An electrical signal is sent from the brain activating hamstrings to provide force and motion, resulting in a muscles measurable activation energy. This activation energy increases in the hamstrings when the ACL is torn as ACL strain causes neural signaling to hamstrings to act, which gets disrupted.

We need actuators to compliment hamstrings physically and electrically. Soft actuators are preferred as they provide looser constraints during multi-axis actuation, which is much safer in case of a failure. Exoskeletons can be used but for weight unloading capabilities (for soldiers, manual workers and aged patients) and not for knee stability or ATT (Pamungkas et al., 2019). Actuated knee brace can provide improvement in daily activities of ACLd patients and help during the critical rehabilitation phase after the ACL injury/surgery.

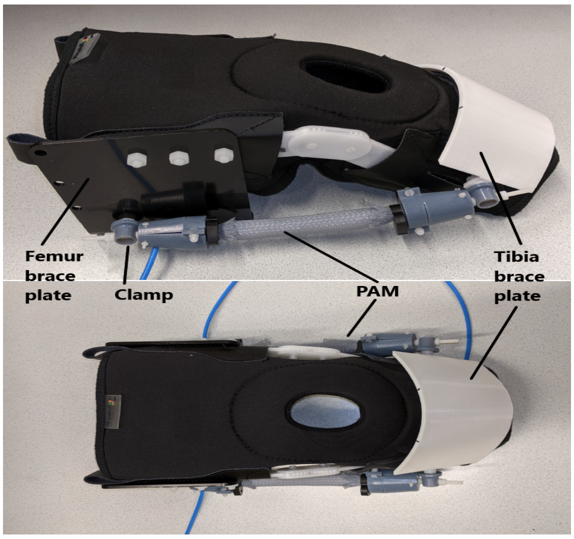

Figure 1.2: Lateral and Top view of the Knee Brace. PAMs are integrated using clamps on femur and tibia brace plate. The light blue pipe is connected to the air pressure pump. (Khambati, 2019)

The modified knee brace (Fig. 1.2) has Pneumatic Artificial Muscles (PAM), which act as soft compliant actuators and is a viable replacement of muscle due to similar energy density. They are capable of providing strain only along their length like normal muscles. These are attached to either side of the femur and tibia plates, respectively, near the knee joint. PAMs can give force distribution in 3-Degrees of Freedom (DoF), making it a good actuator for control compared to most actuator-based exoskeletons having rigid 1-DoF knee support.

Usage of commercial knee brace to help stabilize the ACL deficiency in the knee has been explored (Khambati, 2019). The possibility of PAMs usage was explored in previous studies and used in a knee brace to support the knee and avoid instability.

1.1 Problem Statement

PAM provides the extra forces and constraints required to reduce ATT. Studies have shown that ACLd patients have increased activation energy of hamstring muscles, which can be complemented by changing force generated by PAMs at different knee flexion angles. A model is required to simulate the effects of PAM actuated knee brace on the hamstring muscles group. This needs a musculoskeletal model that can simulate the PAM and knee to see the changes in hamstrings' activation energy under different loading conditions.

1.2 Research Question

How to manipulate hamstring muscle activations, using a soft pneumatic actuator based knee brace, to improve knee gait for ACLd patients?

From the above question, it can be divided into:

1. Compare human knee muscle activations with a PAM actuated brace attached to the knee.

2. Validate the experimental results of PAM brace actuations during walking gait.

3. Modify and control hamstring muscle activations using PAMs.

1.3 Methodology

The target of this research is to study the usage of soft pneumatic actuator based knee brace to control hamstring muscle activations for improving knee gait of ACLd patients.

This research question is achieved by breaking it down to following goals:

- Developing a model to simulate the human knee muscle activation with a PAM actuated brace.

- Comparing simulation and experimental results of PAM brace actuations on hamstrings during walking gait.

- Controlling hamstring muscle activations using PAM actuation.

The heart of the project is generating a model of the knee joint attached with a PAM actuated brace. This could help to check the possibility of using a PAM actuated brace in supplementing hamstring muscles (Khambati, 2019). This would help in understanding the internal workings of the knee which cannot be directly measured. To start with, different models will be explored, tested, and then be included as per need.

The model will need muscles, ligaments, and bone details to target hamstring muscle activations and possibly ATT. Then the brace, and actuators will be integrated into the model for simulations. The behavior of PAM needs to be modeled properly for actuation force and speed. Simulated results will be compared with the data available with previous studies to determine the accuracy of our simulation. Upon reaching a model with sufficient accuracy, different PAM placements and actuations would be tried to control the hamstrings.

The onset of ongoing pandemic COVID-19 has imposed restrictions on collecting new data by conducting experiments and further testing control strategies by implementation on a physical setup. Thus, the controller has become rudimentary and we have to restrict our focus on forward dynamic simulations based on sensor data from previous experiments and simulations. The background literature is in line with the original plan to put the project in physical terms by use of sensors and actuators. But pandemic changes the focus to the modeling aspects of the problem statement.

1.4 Thesis Outline

The thesis follows the following structure:

Chapter 2 - **Background and Literature review** - Checking the knee experiments to detect and measure ACLd. Comparison and selection of the sensors and actuators used in experiments and modeling. Selection of knee model to be used.

Chapter 3 - **Muscle and Neuro Musculoskeletal Models** - Musculotendon model for simulating muscle activations with a NMM targeting knee joint in Opensim. Modifying the selected model to include the knee brace while maintaining the integrity of original experiments and simulations.

Chapter 4 - **Simulations of PAM actuated brace** - Simulations of the modified model with PAM actuated brace for walking gait at different PAM actuations. Validation of simulations with previous experiments. Knee brace having different configurations involving single or double PAMs on each side.

Chapter 5 - **Controlling Hamstring Activation using Dynamic Actuation of PAMs** - Controlling the PAM actuations over the gait cycle for targeted reductions in hamstrings.

Chapter 6 - **Conclusion** - Conclusion and future recommendations.

2 Background and Literature review

The knee joint is one of the most studied joint responsible for our locomotion. It is highly susceptible to injury and wear-tear. To define and understand the knee joint we need to define the components it comprises.

Fig. 2.1 shows the three main bones, femur, tibia, and fibula, which are part of the knee. In the knee joint, the meniscus, patella, and ligaments provide support while hamstrings and quadriceps actuate the joint (Fig. 1.1). Different axis and Degrees of Freedom (DoF) are defined for the kinematics between muscles and bones as shown in Fig. 2.1. The plane of knee joint flexion/extension is in the sagittal plane. And the muscle location is defined using lateral-medial axes.

Hamstrings and quadriceps muscle groups help in flexion and extension of the knee. Similarly, the meniscus is important in the load distribution of force between the femur and tibia. Meniscus also provides secondary constraints when ligament deficiency occurs.

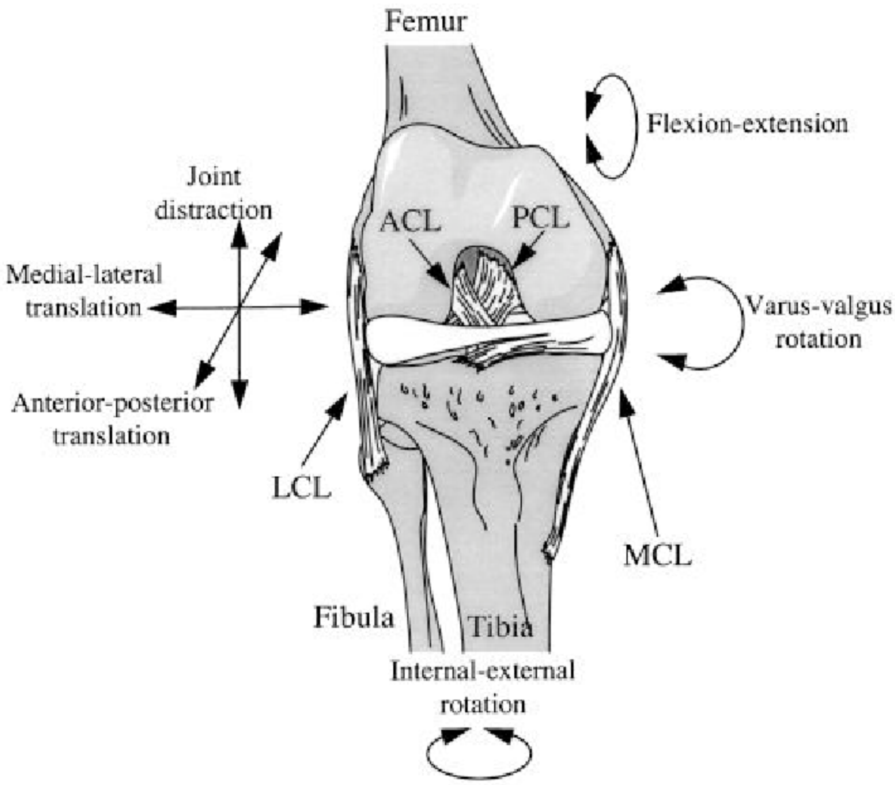

Figure 2.1: Medical terms for different axes of 6-Dof knee Joint. Frontal view of right leg knee without patella. Movement on Anterior-Posterior Axes is Anterior Tibial Translation calculated with respect to patella location. Flexion-extension or knee-rotation axis is the main axes with largest range of motion compared to others. (Subit, 2004)

2.1 Effect of ACLd on Knee joint

During motion, hamstrings provide the majority of force required for knee flexion. Quadriceps are the extensors required to extend the knee. The four ligaments attached around the knee are Anterior-Posterior Cruciate Ligaments and Medial-Lateral Collateral Ligaments. Ligaments provide support and restrictions to these primary motions. The deficiency of one of these ligaments causes instability, meniscal tears, and articular cartilage damage affecting daily life activities. The most susceptible to rupture or injury is ACL (Marieswaran et al., 2018, Makhmalbaf et al., 2013) making it the most studied ligament of the knee joint.

2.1.1 Increased Anterior Tibial Translation

ATT is defined as the gliding of the proximal tibia anteriorly compared to the femur. This ATT motion can further damage meniscus cartilage. For weight-loaded knee extension, especially between 0-30°, quadriceps apply more force than hamstrings causing more ATT (Shelburne et al., 2005b). The mean ATT was lowest to highest in ACLr knees using a bone–patella tendon–bone autograft, ACLr knees using a hamstring autograft, contralateral healthy knees, healthy knees, ACLr knees with an allograft, and ACLd knees (Keizer and Otten, 2019).

The medial collateral ligament was the primary restraint after ACL rupture for ATT (Shelburne et al., 2005a). To check the deficiency of ACL, laxity tests are performed by clinical professionals (App. B). Due to ATT, hamstrings start elongating without neural activation but produce passive strain force.

2.1.2 Changes in hamstrings and quadriceps muscles

Quadriceps avoidance happens when an ACLd patient tries to compensate for the knees stability with slower motion and stiffer joint to avoid using quadriceps muscles. Reducing quadriceps force or quadriceps avoidance was insufficient to restore ATT to the level of an intact knee (Trepczynski et al., 2018). An increase in the level of hamstrings activation accompanies with a decrease in the magnitude of knee extensor moment because of quadriceps avoidance (Shelburne et al., 2005a). This leads to the weakening of quadriceps muscle which makes hamstrings facilitation strategy more favorable than quadriceps avoidance for stabilizing patients with ACLd.

Co-contraction of both the quadriceps and hamstrings theoretically produces zero tension in the ACL at knee angles greater than 30°of flexion. Hamstrings activation generally decreases the ACL load, most notably as the knee is flexed 60-90°(Neumann, 2010). For both normal and ACLd walking, the resultant force acting between the femur and tibia remained mainly on the knees medial side (Shelburne et al., 2005b).

The hamstring muscles can compensate for the instability of the ACLd knee during daily living activities. During late swing and early stance, ACLd individuals demonstrated significantly greater activity in hamstrings as compared to healthy individuals. When hamstrings force reached 56% of its maximal isometric force, ATT was reduced to a near-normal level but causes an increase in forces generated by quadriceps (Liu and Maitland, 2000). This co-contraction leads to stiffer joints and inefficient knee motion.

2.1.3 Neural Delay in Muscle Activation

ACL rupture delays the neural command, leading to a mismatch in the hamstrings and related muscles' activation energies. This delay causes hamstrings to activate more and lead to fatigue. When ACL is tensed, it sends a signal to the hamstrings (not quadriceps) to contract to reduce ACL load (Solomonow and Krogsgaard, 2001). After rupture, the signal delay is >100 ms compared to the normal time of 53 ms. This was seen in both patients with ACLd and ACLr. This delay in signal leads to higher strains in the ACL and hamstrings. With the reduction in hamstrings strength, ACL loading increases by 36% (Weinhandl et al., 2014).

2.2 Sensors

Our focus is on gait recovery for patients with ACLd without graft surgery. Laxity tests (App. B) serve as starting points, but we need continuous sensing and detection methods to understand these tests better. Magnetic Resonance Imaging (MRI) and X-Ray Computed Tomography (CT) are used to measure the severity and damage of ACLd. It also provides the measurement of ATT. These are radiation-based techniques that are unwanted (App. B), as they are not suitable for capturing dynamic movement such as self-paced walking or running.

ACLr surgery is avoidable and can be tracked non-invasively by sensing muscle activations and knee movement. A survey of different sensing units used for assisted walking (Zhang et al., 2019) shows the type of sensors preferred. Surface Electromyography (sEMG) and Inertial Measurement Units are considered the best sensors for calibration and deployment. They can be scaled up for calibration or scaled down for active assistance with ease. We are focusing on a model recreated using EMG signals and joint kinematics to calculate joint forces and moments.

2.2.1 Muscle Activation

Surface Electromyography is a technique where electrodes are placed over the skin, above the targeted nerves and muscles, to study their electrical activity. Since it is placed over the skin and not into the skin through the piercing, it does not hurt and is preferred for its noninvasiveness.

The sEMG uses Al/AgCl circular surface electrodes to detect the electrical potential produced from a superficial muscle when the muscle is in rest, self-contraction, or forceful contractions. sEMGs provide information for muscle activations, which is used to find muscle forces and check muscle dynamics.

With EMG, it is possible to get electrical potential difference produced by muscles during activation ~30 ms before the force is produced. These signals activate the muscles to perform strain action. This early data on the intent of the motion is helpful for feedforward control. The sEMG signals suffer from a high signal to noise ratio. It is also highly dependent on muscle fatigue and the condition of the skin. For each patient, new calibration needs to be done, sometimes more than once. sEMG data is used to record signals from soleus, gastrocnemius, tibialis anterior, vastus lateralis, vastus medialis, rectus femoris, semitendinous, long head of biceps femoris, and gluteus maximus (Shelburne and Pandy, 2002) for lower extremity model, which is required for knee analysis. EMG gives more subject-specific data helping in determining the contribution of different muscles for a defined motion.

The hamstring muscle group consists of Biceps Femoris Long Head (BFLH), Biceps Femoris Short Head (BFSH), SemiTendinosus (ST), and SemiMembranosus (SM), out of which BFLH and ST are superficial muscles. As shown in Fig. 2.2, the biceps femoris are lateral hamstring muscles while others are medial. Due to muscles overlapping nature, it is difficult to detect muscle activation of internal muscles Semimembranosus, and the biceps femoris short head with sEMG. The electrodes were placed on the belly of ST and BFLH muscles. To avoid cross-talk signals being generated, the paired electrodes were placed 10 mm apart.

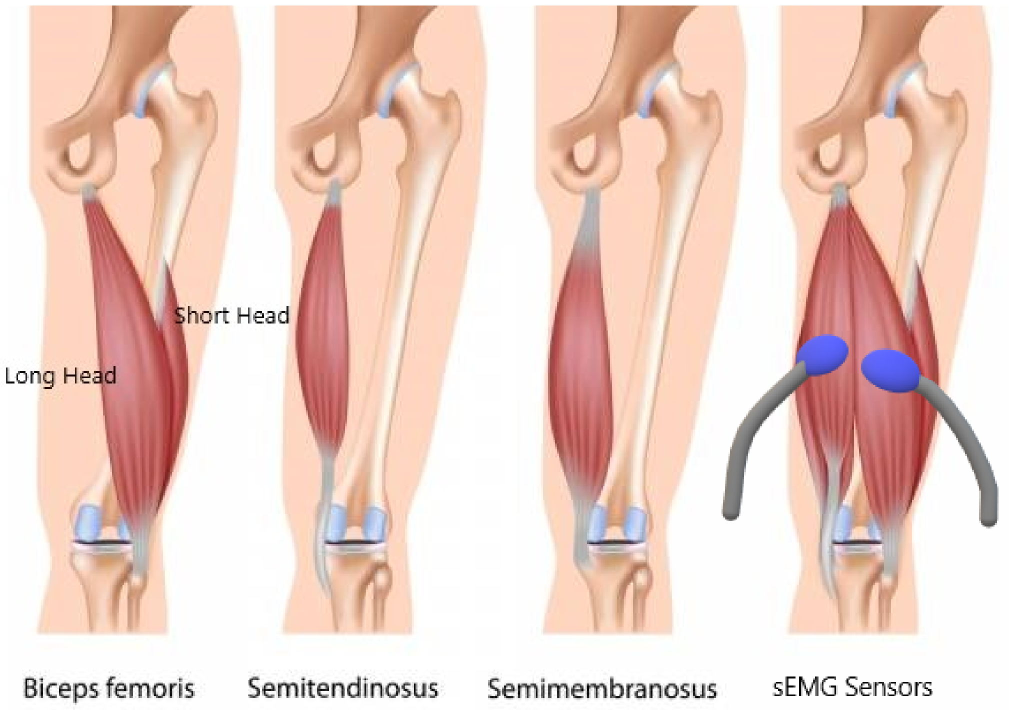

Figure 2.2: Dorsal view (backside) of right leg hamstrings muscle group. Biceps femoris long and short head are lateral hamstring muscles. Semitendinosus and semimembranosus are medial hamstring muscles. sEMG sensors are located on BFLH and ST.

2.2.2 Inertial and Force data

Inertial measurement unit gives inertial data, which is used to measure linear and angular acceleration. This provides us with the kinematic data required for the calculation of joint moments and joint reaction forces. Sensors to collect motion data are discussed in App. A. Due to integration, the signal can generate bias and is useless when the subject is still, yet muscles are tensed consciously. Sensors are widely used in active braces (Bravo-Illanes et al., 2019,Pamungkas et al., 2019) and exoskeletons (Parween et al., 2019). With these data acquisition methods, a model can be created to identify and recreate the interactions between the different bones, muscles, ligaments, etc.

2.3 Pneumatic Artificial Muscle (PAM) Actuator

Pneumatic Artificial Muscle is a fluid-based soft actuator, also known as the Mckibben actuator (Kang et al., 2009). They are called artificial muscles due to their soft compliance and energy density being similar to muscles. PAMs are lightweight and have a high force to weight ratio comparing with electrical motors. They only contract to provide a pulling force and respond quickly to loads through the midsection compared to endpoints, like muscles. The fluid used is normal air making it completely safe in any operational situation. Air compressibility also plays a cushion role against unpredictable impact.

Being compliant and air-based makes the PAM 6-DoF actuator with a major 1-DoF line of action. It is easier to model PAM during actuation when there are no other restrictions to bulging (Khambati, 2019). Inherently PAMs are non-linear systems (Lappas, 2020) and get difficult to model if wrapped around surfaces. They are preferred to be used in assistive devices to help injured, and disabled people perform normal daily living activities.

PAMs are cylindrical fluid based compliant actuators. They have an inner thin membrane that is connected to a pressure pump. On the outer side, a strong interwoven fiber allows the bulging of the inner membrane to be restricted. Stiff endpoints take the strain of bulging. These endpoints are rigidly attached between the objects requiring such actuation force. The pattern of fiber defines the properties of the PAM like actuation length and force generated. PAMs have higher energy density when compared to traditional mechanical actuators. They are safer to operate as they do not overdrive if strained beyond operational limits.

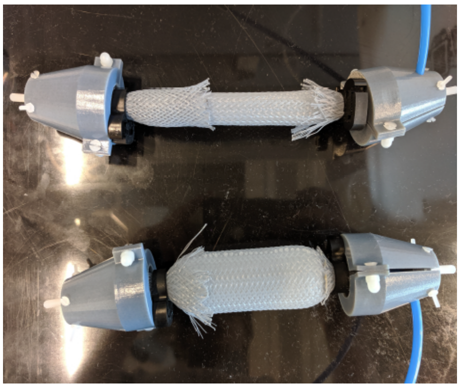

(a) Top PAM is unactuated and bottom is fully actuated. Both are without restraints

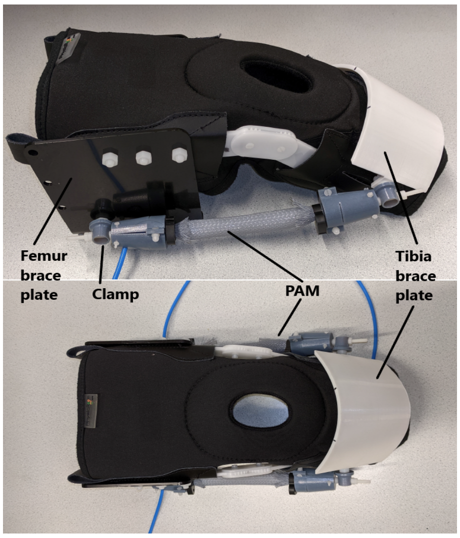

(b) PAMs integrated on femur and tibia plate with clamps having free rotation in sagittal plane

Figure 2.3: 3D Printed PAMs and PAM based brace

Above Fig. 2.3a shows two PAMs, one actuated and one unactuated, in free mode without any restraints. The actuated PAM has a shortened length and bulging center. In Fig. 2.3b PAMs are attached to the femur and tibia plate on both sides of the brace. The brace allows knee rotation from 0-90°, sufficient for normal walking. An Arduino UNO microcontroller board was used to actuate the PAM and air pressure is controlled by a FESTO 2 bar pressure regulator. 1bar is considered a safe limit for operation. The speed of PAM actuation can be varied with frequency, but it leads to a reduction in actuation range for frequencies beyond 20Hz for 0-1bar pressure range.

2.4 PAM actuated knee brace

Assistive devices such as exoskeletons, braces, etc., are developed for pre/post-surgery. Exoskeletons are mostly developed for immobile patients, warehouse workers, and army soldiers, as it helps to unload the full weight through the ground plate below the feet. It has a rigid structure that does not provide sufficient flexibility, restricting the hip, knee, and ankles finer motions. These limitations and price constraints make knee braces more lucrative as compared to exoskeletons for the general population helping in daily activities.

Functional braces have been able to reduce ATT but only in non-weight bearing activities (Beynnon et al., 2003). Braces are expected to provide support to the knee and avoid ATT. This is done by soft restraints helping to avoid damage during knee motion. Common passive and active (2-DoF) braces (Fleming et al., 2000) do not help in internal-external torques or varus-valgus moments. Braces that help in anterior tibial displacement but causes a delay in reaction time of hamstring muscles (Fleming et al., 2000, Torry et al., 2001). Braces restrict the motion and cause a delayed co-activation of hamstrings, which is an adverse effect as it increases the delay in neural signal due to ACL tear. Non-invasive sensors like sEMG allow them to be attached to the knee along with the brace to check the neural excitation of nearby muscles. EMG signals are used as input to drive the brace (Lyu et al., 2019). Such brace is developed for lower extremity motor disability in adults.

A PAM-based knee brace (Fig. 1.2) is being developed at Robotics and Mechatronics Group at the University of Twente, Netherlands. It uses a commercial knee brace design modified to accompany sensors for the detection of knee flexion angle. PAMs with integral sensors exist but makes the brace MRI incompatible. The soft pneumatic actuators use plastic 3D printed clamps to make knee brace compatible. The sensors are currently removable but not compatible with MRI/CT.

PAM actuated brace is supposed to mimic and complement the function of hamstrings during walking. Fig. 2.4 shows the contribution of hamstrings, ACL, and the proposed knee brace on knee stability for different conditions. The experiments are performed (Khambati, 2019) to check the effect of PAMs different actuation forces as various load conditions.

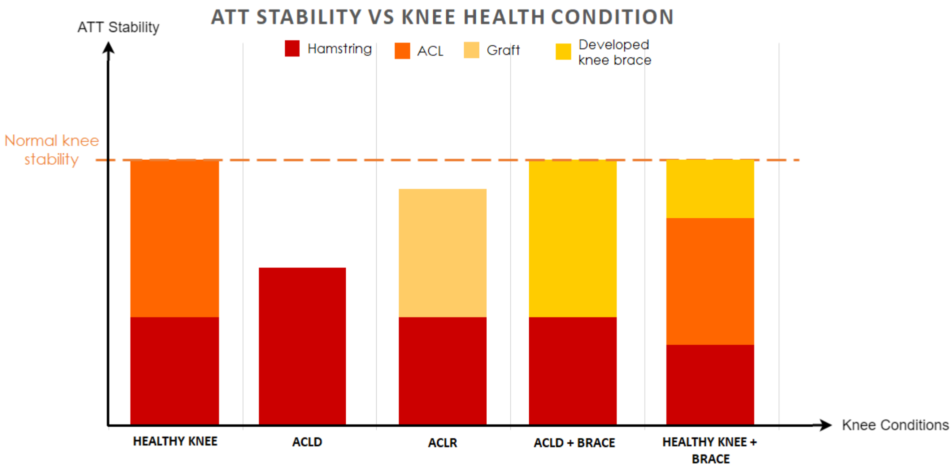

Figure 2.4: Contribution of ACL, hamstrings and knee brace is compared for different knee health conditions and ATT stability (Khambati, 2019)

The PAM actuated brace (Khambati, 2019) used for experiments was a commercial fabric brace reinforced with PLA brace plates to attach PAMs. To measure sEMG signals of hamstrings, firstly, a static test (biceps curl) was done to determine the Maximum Voluntary Isometric Contraction (MVIC). MVIC of individual muscles is used to normalize EMG signals. Experiments involved 3 participants walking at normal gait speed wearing the PAM actuated knee brace. The hamstring muscle activations were collected using sEMG for different PAM actuations. The raw signal collected from electrodes is amplified using an amplifier (Micromed MATRIX Light) as shown in Fig. 2.5. This amplified EMG data was then evaluated with a Micromed software, system plus, which records and visualizes the EMG data signals. It is also important to do frequent calibrations since the sensors move along the skin/fabric.

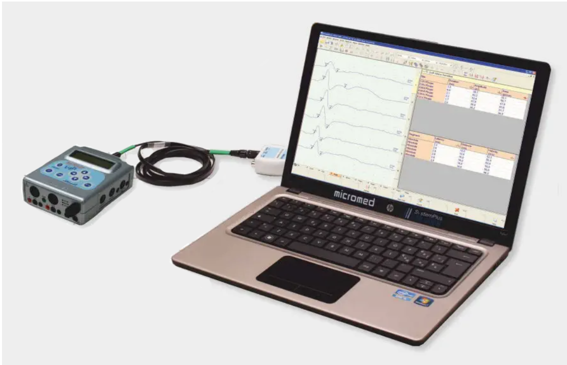

Figure 2.5: 2-Channel sEMG setup with MATRIX lite (Matrix Website)

The report (Khambati, 2019), shows the experiments conducted using the PAM brace during walking gait. It uses different force actuation and sEMG sensors to check its effect on hamstring muscle activations.

As per the initial problem statement, a physical setup was tested and made operational for movement in the Robotics and Mechatronics (RAM) lab. However, this setup became inaccessible due to the Covid-19 pandemic. Because of which we had to shift our focus entirely on simulation. Also, we were restricted to use the data available from previous experiments as we couldn't generate our own data through experiments.

2.5 Knee Joint Models

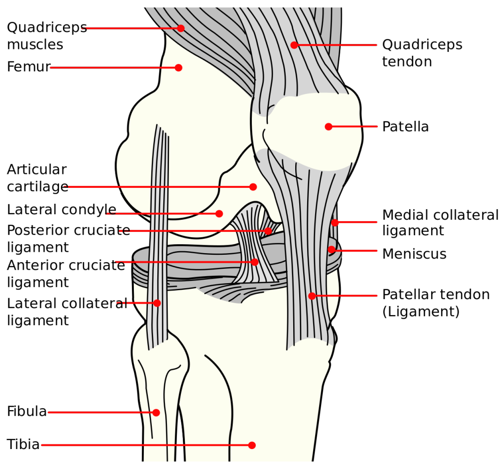

(a) Exploded view of knee joint showing the location of ligaments, bones and tendons. (Wikimedia, 2008)

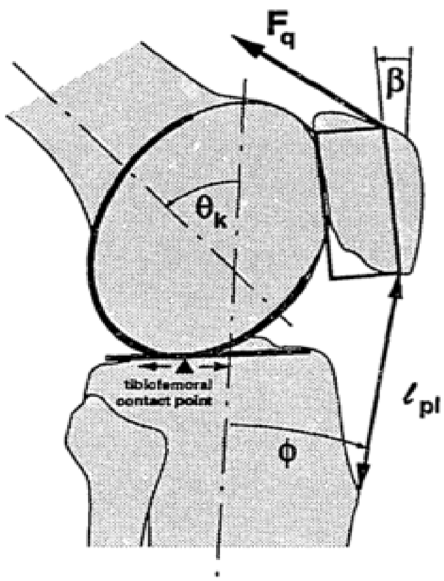

(b) Geometry for calculating kinematics in the sagittal plane. θ_k is the knee angle; ϕ is the patellar ligament angle; β is the angle between the patella and the tibia; F_q is the quadriceps force; ℓ_{pl} is the length of the patellar ligament. From these kinematics, muscles' forces and moments about the instant center of knee rotation can be computed. (Delp et al., 1990)

Figure 2.6: Detailed representation of the knee joint and a simplified 2-Dof knee joint

The human gait model requires a detailed lower extremity model concentrating on anatomical structure (bone, muscle, and joint placement). Anatomical dimension values of muscle and bone are required for scaling a model to a specimen specific model. To understand the intricacies of the internal working of the human body and their interactions a model is needed. A generic model is suitable for such purposes. Knee joint models are developed to identify the force interaction between its sub-parts, as shown in Fig. 2.6a. But to recreate a past/possible injury event or for surgery, a patient-specific model is needed.

2.5.1 Musculoskeletal Model

As seen in Fig. 2.6b the forces are linearized for simplicity. This simplification allows us to measure moments and forces generated by different muscles and joints. Older 2D planar models were used for such purpose (Yamaguchi and Zajac, 1989, Delp et al., 1990). Such models included muscle contraction dynamics but were passive musculoskeletal models used for calculating joint forces and moments under isometric conditions (Hoy et al., 1990). Using a multi rigid body simulation framework gives the flexibility to modify the model for greater detail and accuracy as per the information.

Still, it is not a good imitation of an actual knee. For proper mechanical modeling with all soft tissue properties, Finite Element Models (FEM) are used. The FEM is made using MRI and CT scans of the patients. FEMs are usually used for surgeries involving implants or meniscus cartilage before ACLr (Nikolopoulos et al., 2020). To model ligaments and meniscus, it is common to use finite element simulation for load distribution. FEM of the knee (Nicolella et al., 2011, Naghibi Beidokhti et al., 2016) are detailed mesh-based models focusing on ACL deficiency and reconstruction. These models can provide accurate information on expected loads during walking at different points on ligaments, meniscus, etc. It is difficult to verify the actual hamstring forces in the knee during dynamic activities using high fidelity sensing techniques. Such sensors are usually invasive. Thus, model modifications are made using MRI and CT scans of patients. The calculated joint contact forces in ACLr patients were higher than in healthy subjects (Trepczynski et al., 2018).

Neural networks (Ezati, 2019) are used for real-time prediction of human movement. The paper also discusses different musculoskeletal and neuro-musculoskeletal models using Computed Muscle Control, discussed further in Ch. 3. FEM and other models are compared for the effect of injury on knee joint reaction forces (Wesseling et al., 2018, Ezati, 2019). The knee joint coordinates need to have dynamic coupling between nearby ligaments and muscles to properly simulate ACL rupture, tibial rotation, ATT, etc., made from patient-specific data and not for generic dynamic activities. They have a very high computation cost due to the complex and high fidelity model. Such models have a disadvantage for our research as they do not model muscle activation.

2.5.2 Neuro Musculoskeletal Model

Some of the above-discussed models have muscle contraction dynamics but lack muscle activation dynamics due to neural activity. This has to be supported by muscle models capable of changing neural signals from the brain to output force patterns (Seth et al., 2011). These different structures, along with sensor inputs, provide forward simulations of walking gait. This helps to calculate the activations and forces in hamstrings and check for ACL variable constraints or their lack. This is called a **Neuro Musculoskeletal Model (NMM)**. Using the Opensim functions (Sec. 3.5), sensor data, and a model, we can simulate interactions between muscle activations and joint properties in a dynamic environment.

We are targeting the hamstrings muscle group for the effects of the knee brace, but to generate a lower extremity model, muscle activations from other leg muscles are also needed. Out of the modeling techniques discussed earlier creating a NMM is the best path forward in incorporating the data from experiments.

Brief about some of the NMM that were explored is given below:

1. TLEMsafe project (Horsman, 2007, Fregly et al., 2012) by the University of Twente creating a personalized model for healthy gait and gait disorders but is based on Anybody Technology framework which is not an open-source.

2. Subject-specific models in Opensim for patients with Knee osteoarthritis by calculating joint moments for gait modifications but not focusing on muscle activations (Schlotman, 2017).

3. Static pose Lachman test using a detailed model of the knee with ligaments (Stanev et al., 2016, Liu and Maitland, 2000). Developed to model muscle contraction dynamics and not for muscle activation dynamics. It leads to the study of passive ATT only and can not be used to study the walking gait.

4. EMG driven subject-specific (Opensim) model to drive exoskeleton for neurologically impaired patients (Durandau et al., 2019).

5. Co-simulation: NMM includes rigid body dynamics and the force-length-velocity behavior of muscles while tissue mechanics from FEM encompasses the stress-strain behavior of cartilage and ligaments.(Schmitz and Piovesan, 2016).

6. EMG assisted modeling using Calibrated EMG-Informed Neuro Musculo-Skeletal (CEINMS) modeling toolbox (Pizzolato et al., 2015) but requires a large dataset for calibrating the model.

7. Affect on ATT due to forces generated by quadriceps and hamstrings in patients with ACLd and ACLr during walking gait. The model has ligaments (Shelburne et al., 2005a) but is only force-based and not EMG.

Complete lower extremity model with EMG data is not freely available for the above-discussed models.

The data acquisition techniques discussed help in generating a NMM to recreate experiments. The model to simulate walking gait is developed (Rajagopal et al., 2016) using Opensim (Seth et al., 2011). The software helps in developing a NMM to study the effect of PAM on the hamstrings muscle group. Experiments for data collection and modeling were done at the Massachusetts Institute of Technology (Rajagopal et al., 2016) to simulate a muscle-driven model during walking gait.

During experiments, wireless surface electrodes were placed on ten muscles (including BFLH), and EMG signals were recorded for each muscle. To filter these signals, methods like moving average windowing and Butterworth filter were used. For walking gait, the subject walked over the ground at a self-selected speed. Motion data were collected using an eight-camera optical motion capture system that measured 41 retro-reflective markers' marker positions at 100 Hz. Overground force plates were used to measure the ground reaction forces and moments at 2000 Hz. The above-chosen model is described in Sec. 3.2 and its results will be taken as a baseline model for further improvements and simulations.

For further study, we choose the model (Rajagopal et al., 2016) as it is best suited to simulate the PAM actuated brace with its effect on hamstring muscle activations measured (Khambati, 2019) through sEMG for gait cycles (walking) of healthy patients.

3 Muscle and Neuro Musculoskeletal Models

In this chapter, our goal is to find and use the most helpful simulation paradigm sufficient to model the internal working of the human body involving muscles, skeleton, and brain. The modeling technique adopted to create the model in Sec. 2.5.2 is discussed in detail. The chapter starts with details of the biomechanical model of muscles. Then it moves forward to the model developed at the Massachusetts Institute of Technology (Rajagopal et al., 2016) and the properties in its knee model. Following the model, modifications are done to the model for the addition of the PAM actuated knee brace. The framework used to simulate is discussed later in the chapter. This chapter also deals with the goal of developing a model to simulate the interactions of the various components comprising the knee joint.

Muscles are over-actuated systems wrapped around the joints and bones. This causes the body to activate most of the concerned muscles but uses them accordingly for the task at hand. This division of work amongst the muscle groups is a personal calibration based on their age, sex, weight, exercise, work, and other factors, making it difficult to identify healthy muscle activity. Individual muscles in a knee joint have a personalized activity pattern. This requires a patient-specific model of the knee to simulate and check.

A model is needed to examine the various interactions of different muscles and bones in our body. A biomechanical model provides muscle tension and joint contact forces at different joints that otherwise would need invasive methods. A dynamic model uses non-invasive methods like motion capture, force plates, and EMG to get body segment kinematics, ground reaction forces, and muscle activation. Cadaveric experiments (Ali et al., 2017) on patients provide detailed geometric and material properties of cartilage and ligaments used to find muscle model properties. These are obtained through different mobility tests with integrated sensors after surgery and imaging techniques like CT and MRI (App. B). This data leads to developing a highly detailed model. Models developed by medical professionals are specific for surgery, implants, and biomedical-human machine interaction. They are used to, for instance, measure knee implants' effects on the load-bearing and constraint capabilities of menisci and cruciate ligaments.

Using detailed parameters of muscle fibers and joint interactions, a patient-specific model is created. Using such models, complex interactions of muscles are broken down into generic couplings. Such results assist in realizing the general effect of different factors in musculoskeletal behavior. The knee or lower extremity model should have high fidelity yet flexibility to simulate a generic model. The calculated parameters need to be combined with muscle models to provide force distributions among muscle groups and the body. This combination helps to simulate and predict muscle activity. A model that could meet the requirements and provide a solution to achieve healthier knee stability and function is a high-speed generic Neuro-Musculoskeletal Model (NMM).

3.1 Muscle models

Muscle generates force by contraction and does not have the capacity to generate outward force. The contraction rate is much higher than the relaxation rate. The higher the load applied to the muscle, the lower the contraction velocity. Similarly, the higher the contraction velocity, the lower the tension in the muscle. During the slow and fast-twitch reactions, muscle fibers vary in activation time from 5 ms to 40-50 ms. The reaction time depends on muscle activation dynamics. The muscle activation is a first-order differential equation.

$$\frac{da}{dt} = \frac{u-a}{\tau(a,u)} \tag{3.1}$$

u and a are the neural excitations and muscle activation signals; it varies from 0 to 1 scale using the isometric contraction of muscles to calculate muscles' reference activation.

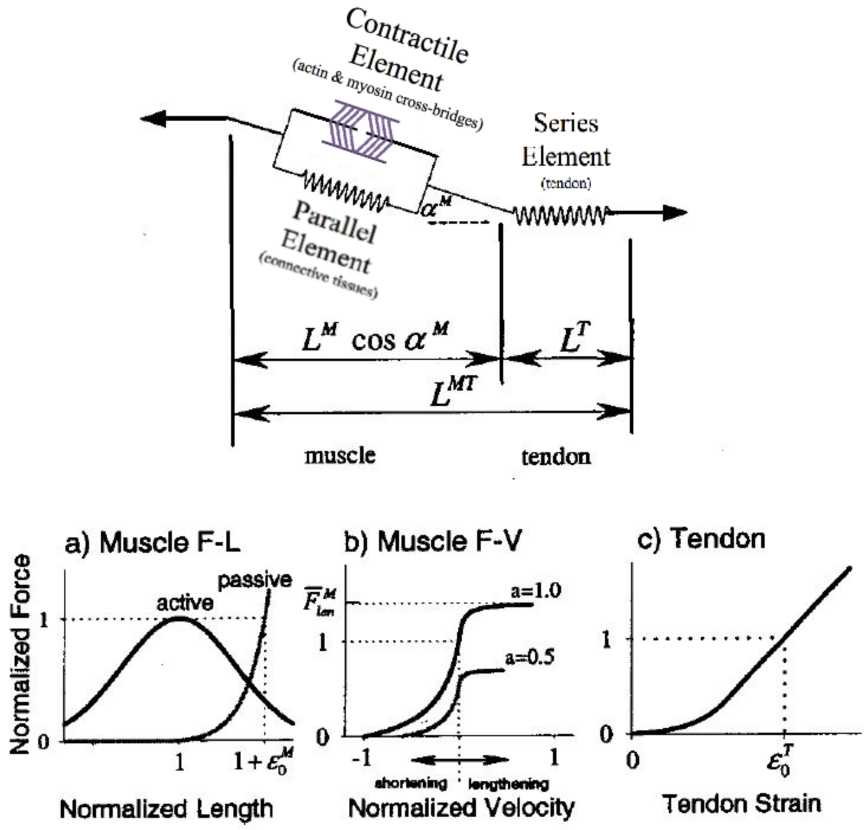

Figure 3.1: 3 Element Hill type musculotendon model. Generalised Muscle Force-length, Force-Velocity and Tendon Strain response. (Thelen, 2003,Battista et al., 2017)

Muscles are modeled as massless linear actuators consisting of passive springs and an active contractile element. They can only produce active inward forces.

The Hill muscle model (Fig. 3.1) represents the muscle's mechanical response.

Hill-type muscle model has this basic structure and four characteristic curves:

1. Active force-length curve
2. Passive force-length curve
3. Force-velocity curve
4. Tendon force-length curve

It consists of a contractile element (CE) arranged alongside a parallel elastic element (PE) and in series with a series elastic element (SE). Force development (F_{CE}) within the CE is a function (k) of activation kinetics (a), force-length (f-l) properties, and force-velocity (f-v) properties.

$$F_{CE} = k(a, f - l, f - v) \tag{3.2}$$

Force developed by the parallel spring depends on the CE length, while force in the SE is equal to the sum of PE and CE forces. PE has soft tissue mechanical behavior and is responsible for the muscle's passive behavior when stretched, even when the CE is not activated. The SE represents the tendon and the intrinsic elasticity of the myofilaments. It also has a passive soft tissue response and provides an energy storing mechanism. It smoothens out the rapid changes in the muscle tension.

Muscle architecture requires physiological data collection from cadavers, such as max. isometric force, pennation angle (α^M), optimal fiber length, muscle fiber length (L^M), tendon slack length (L^T), physiological cross-sectional area, etc. Hill-type muscle models differ based on the characteristic curves and parameters chosen.

Parameters vary broadly in number based on the availability of specimens and measurement techniques. To counter the loss of muscle details due to the simplifications done by assuming a 3-element model, we need an efficient and detailed muscle model. Millard muscle model (Millard et al., 2013) is used for its high fidelity yet computationally efficient muscle model. Using rigid body dynamics and muscle models, we can create a model to simulate human knee dynamics and muscle activations.

3.2 Neuro-Musculoskeletal Model

To model muscle activity and contribution in human motion, OpenSim is used. Opensim provides a framework for musculoskeletal modeling and simulations using various biomechanical joints, muscle actuators, ligament forces, compliant contact, and controllers. Using anatomic skeletal model, hill-type muscle models with multi-body dynamics, a Neuro-Musculoskeletal Model (NMM) is created. This model can be generated using data from the sensors mentioned in Ch. 2. A multi-body dynamics engine, Simbody (Sherman et al., 2011), is used to simulate the model's dynamic equations forward in time. Inverse analysis using this engine solves for underlying kinematics and dynamics.

Muscles are 1-dimensional massless lines acting from an endpoint to another endpoint. Muscles in the body do not act in such a way but wrap around different body segments. Muscles are attached to various bones with multiple path points. This is shown in Fig. 3.2.

Due to the size and complexity of actual muscle groups, the muscle models are divided into smaller muscles connecting different bodies and acting over different paths. Hamstrings muscle group (Fig. 3.2) consists of Biceps Femoris Long Head (BFLH), Biceps Femoris Short Head (BFSH), Semitendinosus (ST), and Semimembranosus (SM). Being a big muscle group, it has different muscle lengths and twitches reaction fibers along with it. Thus, it is suitable to divide. This helps to model the complex behavior of slow, stronger, and shorter fibers in BFSH vs. the faster and longer muscle of BFLH. BFLH being superficial can be measured using EMG, unlike BFSH. The same goes for ST and SM, where ST is superficial compared to SM. BFLH and BFSH are lateral muscles and ST and SM medial. Their unequal actuation causes rotation of the tibia with respect to the femur when the knee is flexed.

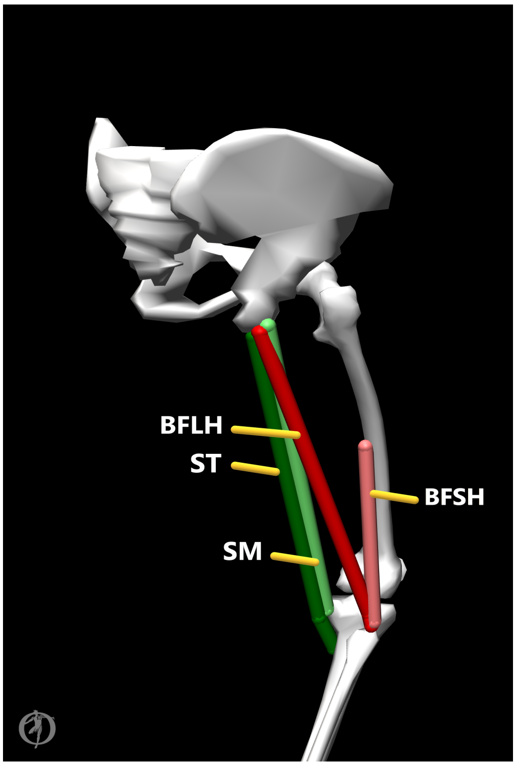

(a) Hamstrings muscle group

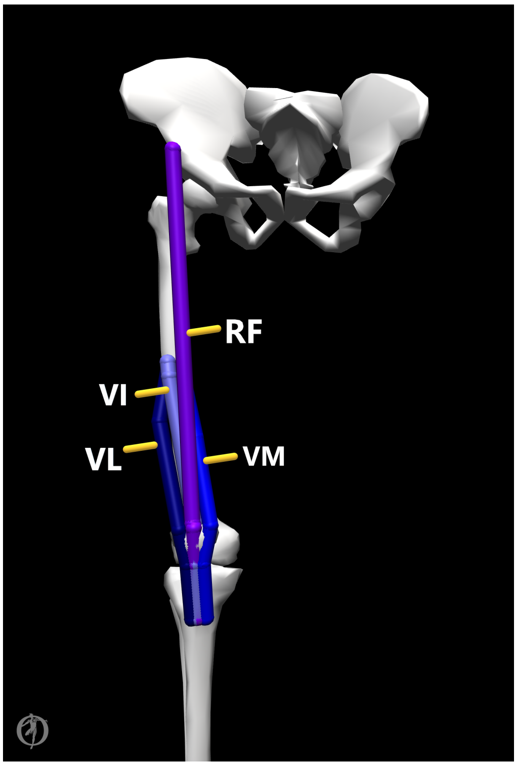

(b) Quadriceps muscle group

Figure 3.2: The muscles are color coded as Hamstrings: Biceps Femoris Long Head (BFLH)-Red, Biceps Femoris Short Head (BFSH)-Pink, SemiMembranosus (SM)-Light Green, SemiTendinosus (ST)-Dark Green and Quadriceps: Rectus Femoris (RF)-Purple, Vastus Medialis (VM)-Blue, Vastus Lateralis (VL)-Dark Blue, Vastus Intermedius (VI)-Light Blue

Quadriceps muscles - Vastus Lateralis (VL), Vastus Intermedius (VI), and Vastus Medialis (VM) join the anterior region of the femur to the upper shin of the tibia. They also wrap over the knee joint by having path points on the patella. Rectus Femoris (RF) starts from the hip bone and follows similar path overlapping VI. With the help of these muscles, femur-tibia motion is stabilized during knee extension. RF is also a superficial muscle like BFLH and ST.

In Opensim, muscles are modeled as an actuator type, which takes neural command or muscle activation as input to generate forces dynamically. A number of such muscles are required to generate a detailed lower extremity model. The model (Rajagopal et al., 2016) shown in Fig. 3.3 is actuated by 80 muscle-tendon units in the lower body (40 per leg) with 20 DoF and 17 torque actuators (one for each DoF in the upper body).

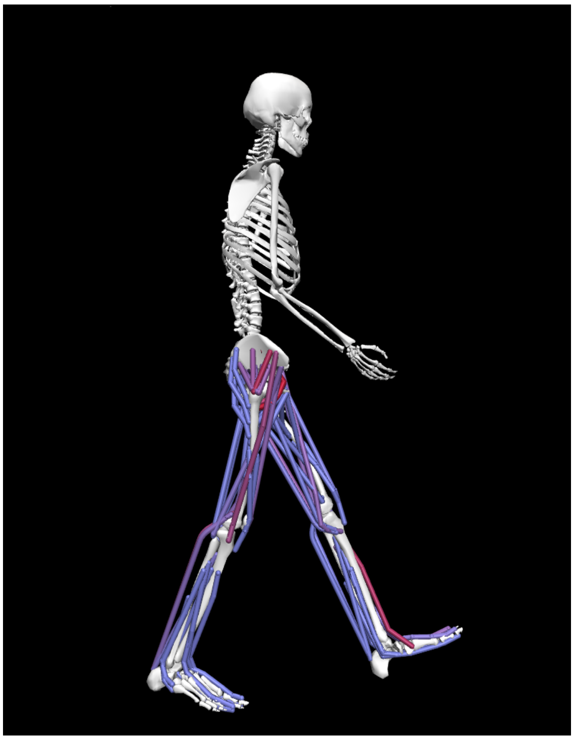

Figure 3.3: Neuro Musculoskeletal Model of Human Lower Extremity for gait

3.3 Knee Model

To model the Brace and PAMs, and attach them to the model, it is required to understand the current knee joint model. Fig. 2.1 shows the 6 DoF of the joint. The main axes are the knee flexion/extension. The knee flexion angle has a range of 0° to 120°. Other axes are modeled as a coupled joint with spline curves with respect to knee flexion angle. This defines the spatial transformation of the joint. Joint distraction is not simulated and is locked. Fig. 3.4 shows the movement range of translations and rotations in other axes of the joint. Increasing knee flexion causes larger motion for Internal-External Rotation and Anterior-Posterior Translation compared to others.

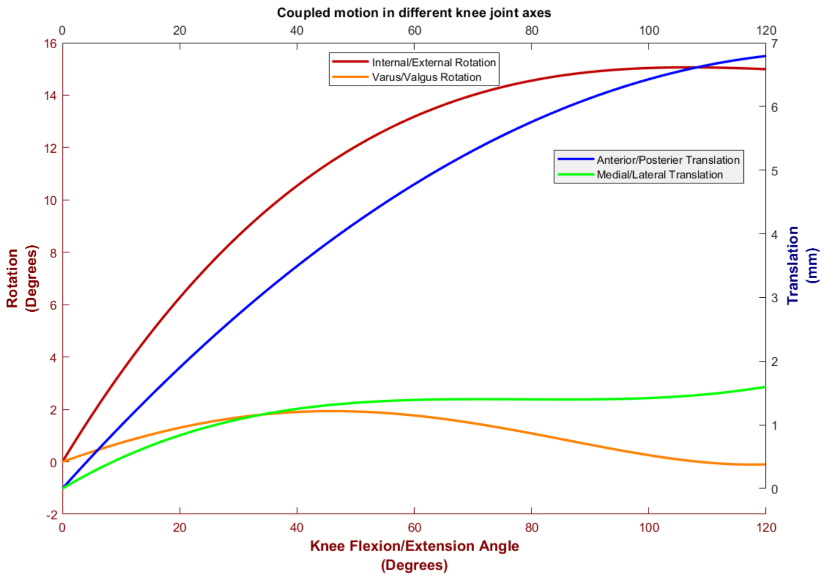

Figure 3.4: Coupled motion of 1-D knee joint axes on Flexion-Extension angle (Rajagopal et al., 2016)

Similarly, patellar kinematics parameterization is on a different axis, as shown in Fig. 3.5a but dependent on knee angle. This dependency is ensured using coordinate coupler constraint.

Fig. 3.5a defines the frames attached to the femur, patella, and tibia. The tibia orientation with respect to the femur was primarily determined by the tibia rotation about the femur-fixed –Z-axis (blue) by the knee flexion angle. The patellar ligament is defined at the quadriceps lines of action to wrap over the patella and insert onto the tibia.

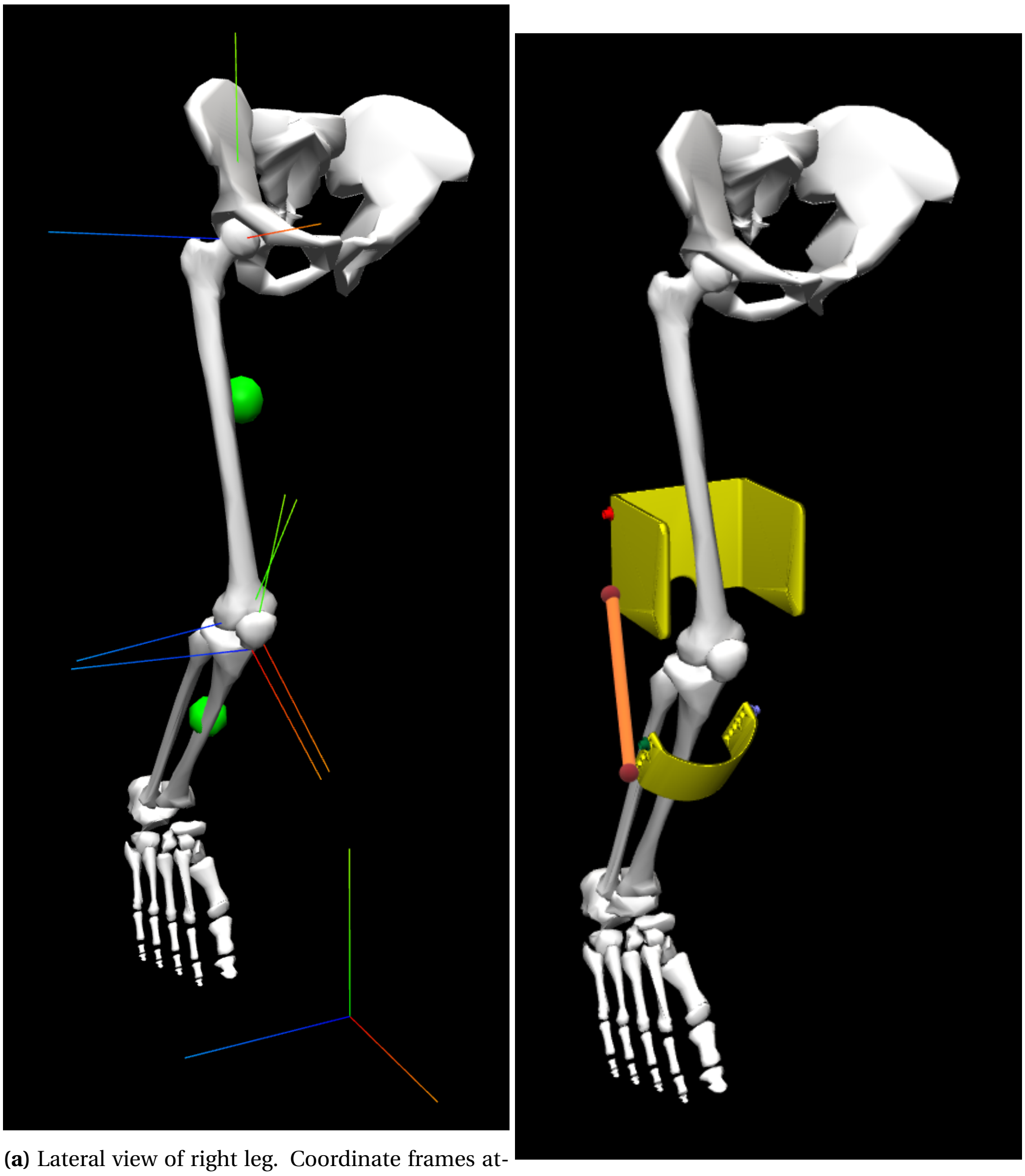

(a) Lateral view of right leg. Coordinate frames attached to femur, patella, tibia and Ground. Center of mass of femur and tibia bone is shown. The coordinate axes are color coded as red (X-axis), green (Y-axis) and blue (Z-axis)

(b) Femur and tibia brace plates (yellow). Attachment points (red) for PAM (orange) at lateral side. Center of mass of brace plates is shown.

Figure 3.5: Lower extremity opensim model with right leg visible (Muscles are hidden)

3.4 PAM actuated brace model

The commercial knee brace (Fig. 2.3b) comprises of elastane textile, which is reinforced with foam pads. To fixate PAMs on a rigid surface, two plates are 3D printed for the femur and tibia. The femur plate covers the hamstrings, while the tibia plate is located below the patella. This configuration allows the PAMs to be attached between the plates allowing higher posterior force to the tibia. The PAM attachment model is shown in Fig. 3.5b. Brace uses a potentiometer to measure knee angle for calculations.

For a braced model, the femur and the tibia brace plates are rigidly attached to the femur and the tibia bone, respectively. Fig. 3.5 shows the center of masses of all four components. The relative motion between the bones, muscles, skin, and brace plates is not modeled. Restrictions in knee motion due to brace are not considered.

A PAM is modeled using point actuators. These point actuators are located on the brace plates at clamping/attachment points (Fig. 3.5b). The mass of PAM is divided among the attachment points (orange in color) on femur and tibia plates. These point actuators point towards each other along the PAMs' (blue in color) line of action to mimic the pulling force.

The excitation signal given to the actuators is based on the knee flexion angle. The PAMs' are actuated between 0-25 N (Khambati, 2019). In the model, the motion along other knee joint axis are not considered while calculating the line of action for PAMs. This leads to an error of 10% in actual actuation along the PAMs axis. There is no restriction on the length of the PAMs. Due to the existence of previous marker data, we can not enforce PAMs force-length constraints between these points. PAM is modeled to provide force ideally for all changes in length during motion. The maximum distance between the attachments is chosen as the relaxed unactuated length of PAM. There is a slack condition in the model to restrict the actuation. During motion, if the length between attachments goes below the max. contracted length (60% of relaxed length), the PAM is considered slack, providing sudden zero actuation. PAMs also don't interact or wrap around the brace plates and muscles.

3.5 Opensim functions

The human body uses the sequences shown in Fig. 3.6 to act or react to its environment. The brain sends a neural command activating the muscles to contract and apply forces. Forces are generated by muscles accordingly to the musculotendon dynamics. These forces when constrained and supported by the musculoskeletal system generates the motion for the body. At this point of observable movement, external forces like ground reaction also affect the final movement of the human body. The sensory organs detect these changing in motion for feedback and send it to the brain. This sequence from brain signals to motion is known as Forward Dynamics. The reverse direction of this flow requires Inverse Kinematics, Inverse Dynamics, and Static Optimization for the calculation of intermediate values.

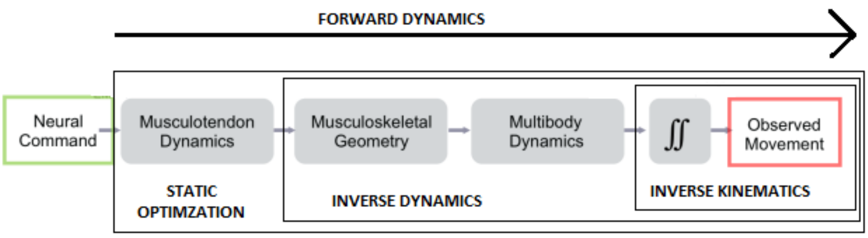

Figure 3.6: Flow of Forward Dynamics based on human body

Using a NMM and following these steps in reverse, we can find all the underlying parameters for walking gait. Movement is reconstructed using Inverse Kinematics and Inverse Dynamics using motion data and contact forces. This is further refined and used as an input for simulating Forward Dynamics.

3.5.1 Inverse Kinematics and Inverse Dynamics

Motion data helps to calculate the position and orientation of all body segments based on markers and sensors used. Motion data is used to calculate physical anatomical parameters required to scale models for segment lengths, mass distribution, etc. Joint kinematics for each motion was computed from motion capture data using the **Inverse Kinematics (IK)** tool in OpenSim4.0.

$$\min_{\boldsymbol{q}} \left[\sum_{i \in \text{markers}} w_i \left\| x_i^{\text{exp}} - x_i(\boldsymbol{q}) \right\|^2 + \sum_{j \in \text{ unprescribed coords}} \omega_j \left(\boldsymbol{q}_j^{\text{exp}} - \boldsymbol{q}_j \right)^2 \right] \tag{3.3}$$

where $\boldsymbol{q}$ is the vector of generalized coordinates being solved for,

x_i^{exp} is the experimental position of marker i,

$x_i(\boldsymbol{q})$ is the position of the corresponding marker on the model for the coordinate values,

$\boldsymbol{q}_j = \boldsymbol{q}_j^{\text{exp}}$ for all prescribed coordinates j as they are not calculated through IK unlike $\boldsymbol{q}_j^{exp}$ in Eq. 3.3.

This optimizes the experimental and model markers for $\boldsymbol{q}, \dot{\boldsymbol{q}}, \ddot{\boldsymbol{q}}$ which are vectors of generalized positions, velocities, and accelerations, respectively. These are used for all further analysis (Fig. 3.7). **Inverse Dynamics (ID)** is defined as

$$\underbrace{\boldsymbol{M}(\boldsymbol{q})\ddot{\boldsymbol{q}} + \boldsymbol{C}(\boldsymbol{q}, \dot{\boldsymbol{q}}) + \boldsymbol{G}(\boldsymbol{q})}_{\text{knowns}} = \underbrace{\boldsymbol{\tau}}_{\text{unknowns}} \tag{3.4}$$

$\boldsymbol{M}(\boldsymbol{q})$ is the system mass matrix;

$\boldsymbol{C}(\boldsymbol{q}, \dot{\boldsymbol{q}})$ is the vector of Coriolis and centrifugal forces;

$\boldsymbol{G}(\boldsymbol{q})$ is the vector of gravitational forces:

$\boldsymbol{\tau}$ is the vector of calculated generalized forces and torques.

These equations depend on the number of DoF of the whole model. There are 37 DoF in the model. 10 DoF represents a leg and 17 torque actuators for the upper body model. The knee joint has 1 DoF for the flexion-extension with other axes dependent on this knee angle. Using this analysis on model, motion, and GRF data, joint torques, and forces are calculated.

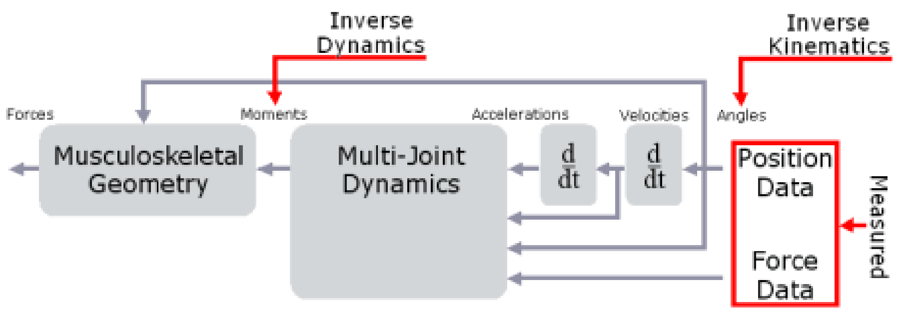

Figure 3.7: Block diagram for Inverse Kinematics and Inverse Dynamics based on measured data. (Odle, 2013)

3.5.2 Static Optimization and Forward Dynamics

Static Optimization (SO) is an extension of ID where it recalculates the muscle activations that produce the dynamics of an observed motion. The new calculation is now subject to actuation and constraints provided by muscles. The model has a total of 80 (p) musculotendon actuators. Since there are more muscles than Dof in the human body, this problem is non-unique and requires optimization. Fig. 3.8b shows the distribution of all the muscles in a leg from the hip to the calcaneus. The muscle activations that produce the dynamics of the motion created by these actuators are calculated. There are more muscle actuators than the DoF, thus it is a non-unique problem and needs optimization. For each time step, the optimization is solved statically for muscle activations.

$$\sum_{m=1}^{p} \left[a_m f\left(F_m^0, l_m, v_m\right)\right] r_{m,j} = \tau_j \tag{3.5}$$

The muscle actuators provide force based on muscle activation (a_m). These forces are constrained by a function (f) of max. isometric force (F_m^0), length (l_m) and contraction velocity (v_m). $r_{m,j}$ is the moment arm for the j^{th} joint. τ_j is the force/torque for same joint.

$$J = \sum_{m=1}^{p} (a_m)^p \tag{3.6}$$

This optimizer minimizes the above summation for muscle activations.

To calculate coordinate accelerations ($\ddot{\boldsymbol{q}}$) joint torques ($\boldsymbol{\tau}$) are input. Rest parameters are the same as ID. External forces ($\boldsymbol{F}$) applied to the model are also included. This is done using FD as below.

$$\ddot{\boldsymbol{q}} = [\boldsymbol{M}(\boldsymbol{q})]^{-1}\{\boldsymbol{\tau} + \boldsymbol{C}(\boldsymbol{q}, \dot{\boldsymbol{q}}) + \boldsymbol{G}(\boldsymbol{q}) + \boldsymbol{F}\} \tag{3.7}$$

SO calculated muscle activations at each instance, which may not be dynamically consistent. To ensure this, differential equations for muscle dynamics are calculated for each discrete time step in the simulation.

$$\boldsymbol{\tau}_{muscle} = [\boldsymbol{R}(\boldsymbol{q})] f(\boldsymbol{a}, \boldsymbol{l}, \boldsymbol{v}) \quad \text{Moments due to muscle forces} \tag{3.8}$$

Net muscle moments ($\boldsymbol{\tau}_{muscle}$) depend on moment arms ($\boldsymbol{R}(\boldsymbol{q})$) and muscle forces. Muscle forces (f) are a function of muscle activation ($\boldsymbol{a}$), muscle fiber length ($\boldsymbol{l}$), and muscle contraction velocity ($\boldsymbol{v}$).

$$\boldsymbol{v} = \Lambda(\boldsymbol{a}, \boldsymbol{l}, \boldsymbol{q}, \dot{\boldsymbol{q}}) \qquad \text{Muscle contraction dynamics} \tag{3.9}$$

Muscle fiber velocities are governed by muscle contraction dynamics (Λ), which depends on the current muscle activations and fiber lengths and the coordinates and velocities.

$$\dot{\boldsymbol{a}} = \mathrm{A}(\boldsymbol{a}, \boldsymbol{u}) \qquad \text{Muscle activation dynamics} \tag{3.10}$$

Activation rates ($\dot{\boldsymbol{a}}$) depend on muscle activation ($\boldsymbol{a}$) and neural excitations ($\boldsymbol{u}$). These equations combined define the muscle dynamics.

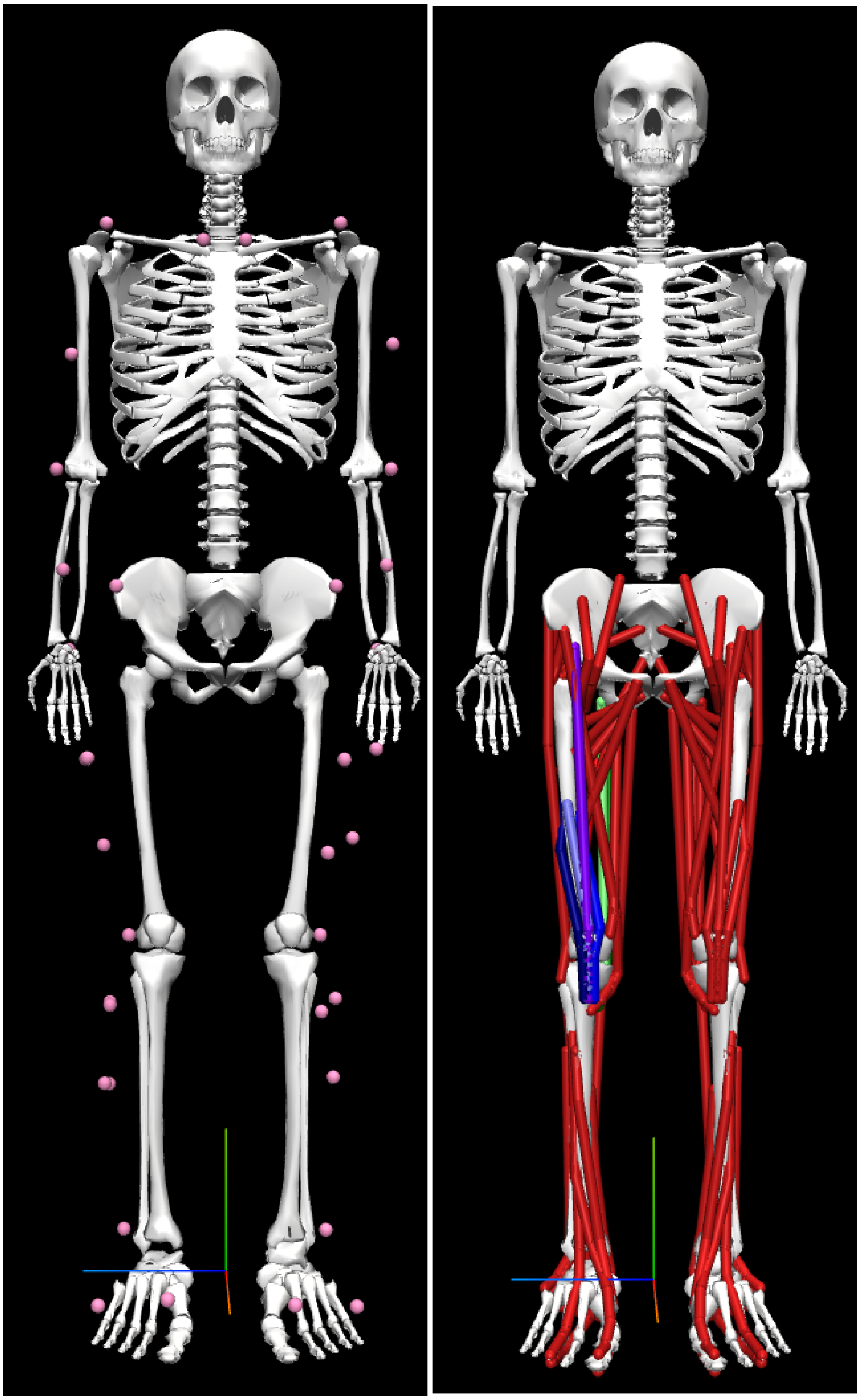

(a) Rigid body model showing human skeletal and markers attached to body.

(b) A complete NMM focusing on representation of human lower extremity muscles.

Figure 3.8: Frontal view of NMM in Opensim with rigid bodies, markers and muscles. The global coordinate axes is represented by RGB colors for XYZ respectively.

Forward Dynamics (FD) is an open-loop simulation using actuator inputs to affect the model dynamically. Being an over-actuated model, information on muscle activations during motion provides better results for the above equations in simulating movement. Without any feedback or desired trajectory, the dynamics are not following a realistic operation. From one instance of time to another, the model variables are dynamically consistent, but they are not realistic.

3.5.3 Computed Muscle Control

Computed Muscle Control (CMC) is used to compute muscle excitation levels that will dynamically drive the model to enforce a desired kinematic trajectory. CMC (Fig. 3.9) uses a combination of Proportional-Derivative (PD) control, SO, and FD.

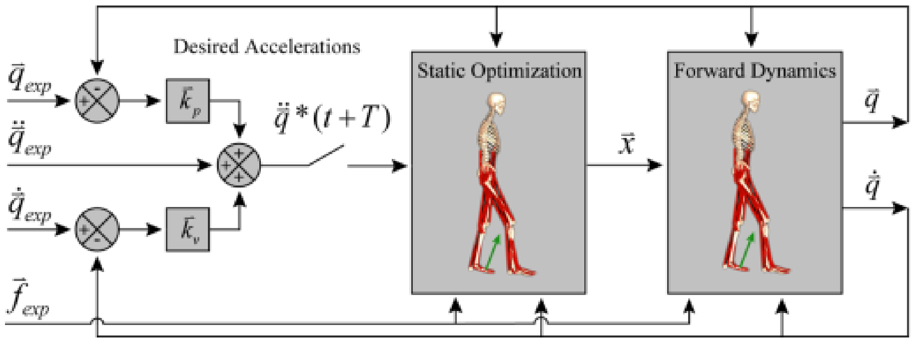

Figure 3.9: Block diagram showing full sequence of CMC. It uses experimental IK and GRF data to calculate SO and FD for desired kinematics enforced by PD controller. (Afonso, 2015)

$$\ddot{\vec{q}}^*(t+T) = \ddot{\vec{q}}_{\text{exp}}(t+T) + \vec{k}_v\left[\dot{\vec{q}}_{\text{exp}}(t) - \dot{\vec{q}}(t)\right] + \vec{k}_p\left[\vec{q}_{\text{exp}}(t) - \vec{q}(t)\right] \tag{3.11}$$

Desired accelerations ($\ddot{\vec{q}}^*$) are computed using PD feedback based on model coordinates ($\vec{q}$) and experimental coordinates ($\vec{q}_{exp}$). Here $\vec{k}_v$ and $\vec{k}_p$ are velocity and position feedback gains for a critically damped response.

$$J = \sum_{i=1}^{n_x} x_i^2 + \sum_{j=1}^{n_q} w_j\left(\ddot{q}_j^* - \ddot{q}_j\right)^2 \tag{3.12}$$

x_i^2 is the actuator control desired to achieve $\ddot{\vec{q}}^*$. SO helps in distributing the load among these actuators. The second summation drives the models unprescribed coordinate accelerations $\ddot{q}_j$ towards the corresponding desired accelerations $\ddot{q}_j^*$. For faster simulations, the second term is considered as a tolerance condition and approximated to zero. This is supplemented using reserve actuators to provide an extra set of lenient constraints for better convergence of the solution. Residual reduction algorithm (RRA) is discussed in App. C to check for simulation validity and possible explanations for the discrepancies during future models and simulations.

The calculated muscle excitations/actuator controls are then used in FD to simulate a prescribed trajectory (experimental data) involving detailed knee NMM during the walking motion.

3.6 Conclusion

A NMM model has been created in OpenSim software with the parameters explained above. Muscles are treated as an actuator in the model and their activation levels are stored in the control states file. The brace plates are attached to the femur and tibia individually. The PAMs are attached to these brace plates without any constraint to their lengths. The PAMs are treated as point actuators with their activation profile manually added to the control states file. This is done to the model after IK and ID calculations. The PAMs are expected to take over the function of the hamstrings muscle group. With SO and FD we have enforced the PAM actuated brace to act as part of the body. This way the model simulations will be forced to follow the IK and ID of normal walking when PAM actuations are given. This should result in a recalculation of muscle contribution with PAM as an additional muscle of the knee joint in SO while running CMC. BFLH and ST are the muscle which was measured (Khambati, 2019) and will be compared with simulation results. The usage of CMC is not the same as controlling the actual knee brace actuations. This is further explored in Ch. 5. Now our model is ready for simulation. We will simulate the model for the self-paced walking of a subject with a healthy knee wearing the PAM actuated brace.

4 Simulations of PAM actuated brace

In this chapter we will be simulating the model with the Computed Muscle Control (CMC) as discussed in Ch. 3. With the attachment of the PAM actuated brace to the knee joint, we can now simulate the effects of PAM actuations on a healthy knee. This would lead to changes in muscle activations and forces generated at the knee joint. These changes will be analyzed with a focus on the hamstrings muscle group. The simulations will be compared with the experimental data available (Khambati, 2019). Later, different PAM configurations on the knee brace are evaluated for their effectiveness in reducing muscle activations in hamstrings. This will provide the best configuration for better manipulation of hamstring muscle activations.

4.1 Gait Cycle

Firstly we need to standardize the experimental and simulation data so that it can be compared. This is done by scaling the data to a 0-100% gait cycle. The cycle describes the leg's gait sequence starting and ending with right leg heel contact (Fig. 4.1).

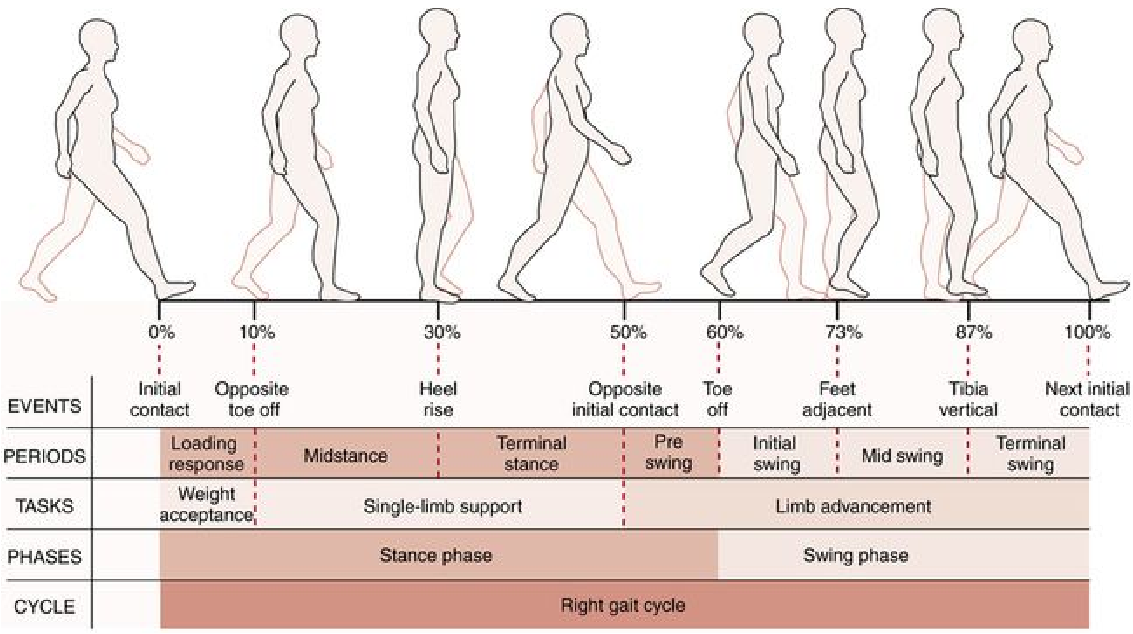

Figure 4.1: Gait Cycle of human walking with respect to heel strike of right foot. (Neumann, 2010)

Using GRF data, we can find the moments at which events like toe-off, heel strike, mid-phase, etc., happen. The following Fig. 4.2 shows the measured ground reaction forces and hamstring muscle activations scaled to gait cycle. GRF is used to adjust the resulting data to start at heel strike which starts at 1.4 s. The model is simulated from 0.48 s to 1.8 s. In which data from 0.56 s to 1.78 s is used and scaled to the gait cycle. In Fig. 4.2a at 1.4 s the right leg strikes the ground increasing the GRF. After 1.78 s the joining of data is done at a point near 25% of the gait cycle, causing some mismatches in muscle forces and activations.

4.1.1 Hamstring muscles contribution

Hamstrings being used for knee flex are not activated during knee extension. This can be seen in Fig. 4.2. For the initial stance phase, the knee starts to flex from initial contact or heel strike event with a maximum contribution at the left toe. With the full load on the right knee, the muscles provide passive forces for support, and the skeletal system takes the main load. The

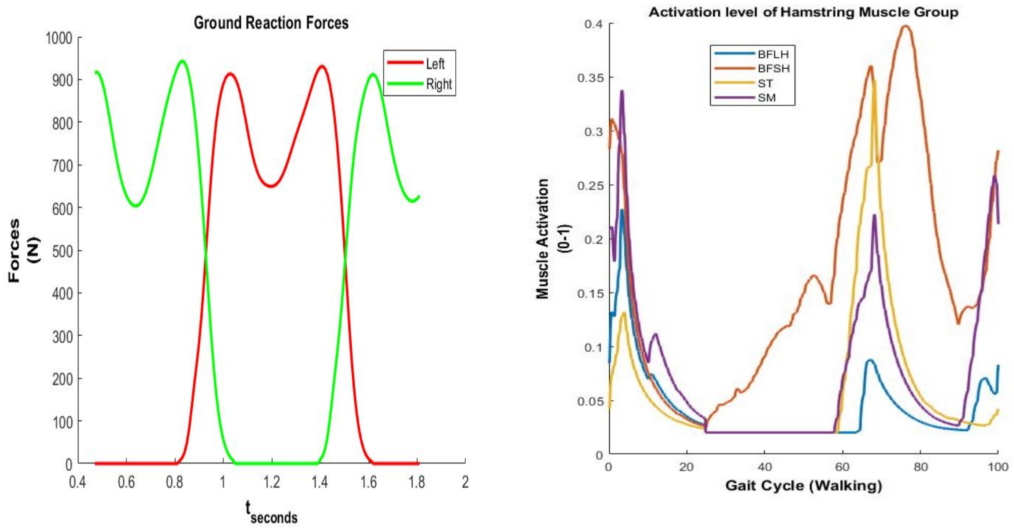

(a) Ground reaction forces during walking

(b) Right leg muscle activation profile (Gait adjusted)

Figure 4.2: Muscle activations adjusted to gait cycle through ground reaction forces (Rajagopal et al., 2016)

knee flexes again at the toe-off event for swing stance and peaks at a point where both feet are adjacent. Hamstrings are activated and providing forces at the starting and end of the gait cycle involving heel contact. These are regions of our interest.

The biceps muscles are not active during 20% to 60% of the gait cycle (Fig. 4.2b) involving weight bearing on the right knee and active from toe-off to the heel strike events. 60% to 90%of the gait cycle (Fig. 4.2b) is the most affected by PAMs. During the swing phase, the brace can decrease muscle activation in hamstring muscles.

Being deeper and inner muscles, SemiMembranosus (SM) and Biceps Femoris Short Head (BFSH) generate the highest muscle forces in the tibia at the heel strike. Although this is a crucial moment for ACL injury compared to knee swing, forces and constraints generated by these do not help in knee joint stability. Thus, it would not be compared further.

4.2 Simulations

The idea of the brace is to provide support to hamstring muscles during walking at different load conditions. Our interest lies in checking the changes caused by the PAM actuations in the hamstring muscles group. Accordingly, hamstring muscle activations can be controlled by our actuation system (PAMs). Out of the 4 muscles, Biceps Femoris Long Head (BFLH) and SemiTendonous (ST) are important.

4.2.1 Effect of knee brace on hamstring muscles

With the simulation, as shown in Fig. 4.3, we checked for the effect of the knee brace's weight on hamstring muscle activations and forces. The brace is attached to the model but is given zero excitation to generate zero actuation.

Due to the weight of braces, there is a slight increase in the muscle forces and activations. The effect is more noticeable in BFLH as compared to ST. During the initial gait cycle, the BFLH has a reduction in activation level, but it has a 5-10% increase in activation and forces in the swing phase. Fig. 4.3 shows the hamstring muscle group's muscle activations and forces before and after the brace is attached to the model.

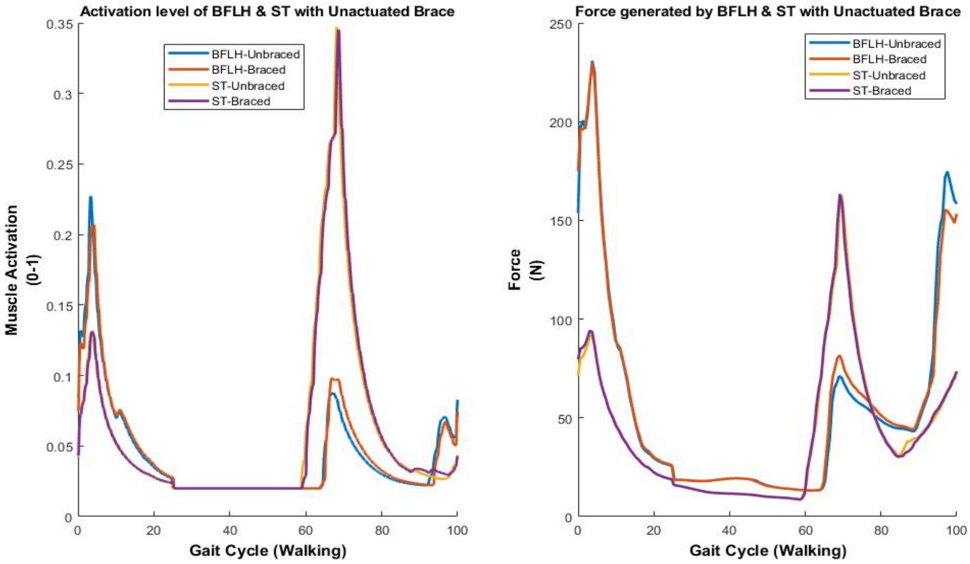

Figure 4.3: Model with rigid body PAM brace attached to the knee joint vs model without the Knee brace

4.2.2 Effect of equal PAM actuations on hamstring muscles

PAM is actuated to provide forces for a reduction in hamstring muscle activations (Fig. 4.4). This reduction could prove the effect of PAM actuated knee brace as being complementary to hamstrings by providing co-activation. Muscle activations for BFLH and ST are checked for different force levels- 0, 10, 20, and 25 N (Khambati, 2019). The maximum actuation of PAM (with force level as 25 N) was calculated using finite element model optimization.

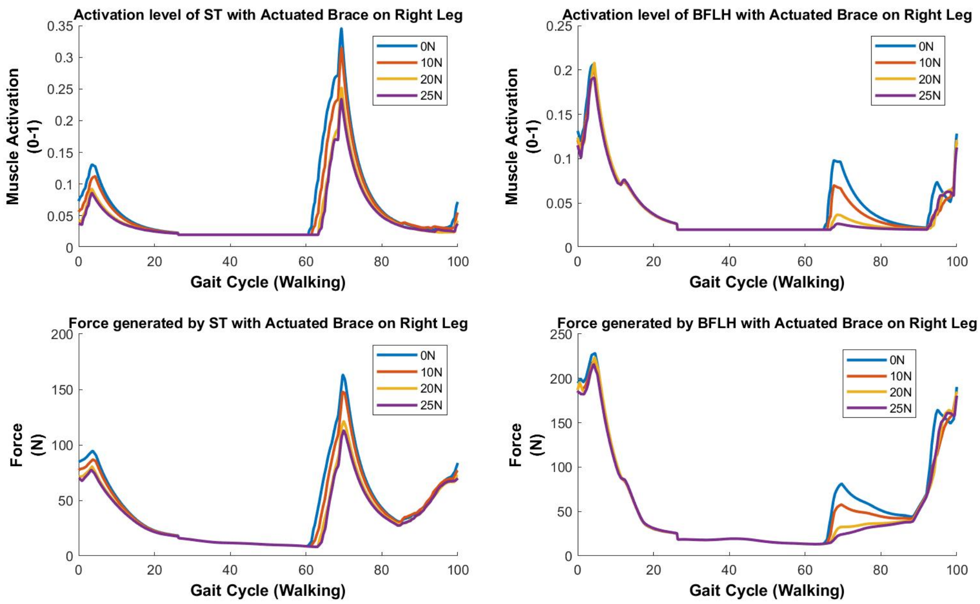

Figure 4.4: Changes in muscle activations and generated forces due to actuated brace

For 68-72% of the gait cycle, the muscle activations reach peak values as shown in the Table 4.1. PAM actuations affect the swing phase more easily than the stance phase. There is a difference in muscle activation and force generated before and after the heel contact event. The

PAM actuation forces	0 N	10 N	20 N	25 N
Muscles	Changes in Muscle Activation Levels			
ST	0.34	0.31	0.25	0.23
BFLH	0.09	0.07	0.04	0.03
	Changes in Forces generated			
ST	163.11	147.02	120.11	111.72
BFLH	81.02	57.72	31.23	23.43

Table 4.1: Comparison of changes in muscle activation with different PAM actuations (swing phase)

force generated could be higher due to the constraints and external forces at heel strike. The difference in activation level for ST muscle during both the initial stance phase and the swing phase is 30%. The decrease in activation with increasing PAM actuation force is easily visible in both. The heel contact event of gait shows more changes for ST instead of BFLH.

4.2.3 Effect of Unequal actuation of lateral and medial PAMs on hamstring muscles

Unequal actuation is given to PAM on the lateral and medial side of the knee brace to check for variation in muscle activations of BFLH and ST. The ratio of actuation is decided based on the contribution of lateral and medial hamstrings (Khambati, 2019). The actuation forces used were 14.5 N for medial and 3.8 N for lateral PAM.

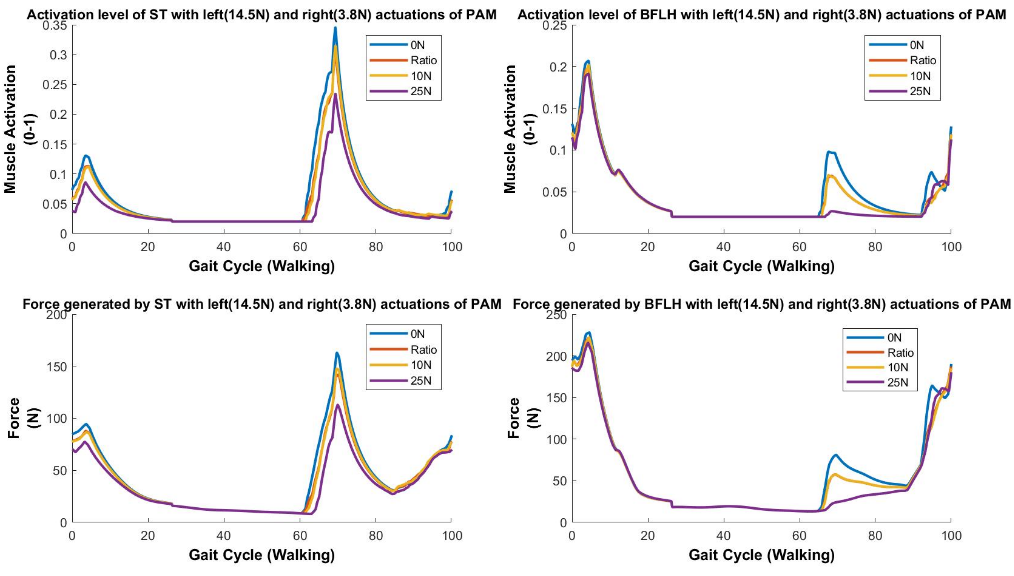

Figure 4.5: Ratio configuration of brace with unequal actuation of left and right PAM

The unequal actuation causes a near-exact effect on hamstrings as if an actuation of 10 N is given (Fig. 4.5). The expectation was to see changes in muscle activations of BFLH and ST. Due to their location on either side of the brace, they should provide unequal torque at the knee joint. No comparable differences in activation levels are noticed because of the limitations in the knee model. The unequal actuation should is expected to affect the brace's rotation. However, it is restricted due to the rigid joint between brace plates and bones. Ratio actuation simulations are currently inconclusive and not reported further.

4.3 Comparing Simulations and Experiments

Now we will compare the data generated through our simulations with the data available through the experiments performed in earlier studies (Khambati, 2019). From here on we are referring to experiments as experiments performed in past studies. With the above simulations, the original conditions of the experiments conducted earlier are recreated as close as possible with available data and resources. The hamstring muscle activations measured in the experiments are compared with results from the simulation of different PAM actuations.

The minimum muscle activation for any muscle is 0.02 on a scale of 0 to 1. Our above simulations show no activation in BFLH during the stance phase, especially during 20-50% of the gait cycle. This is reported as the model limitation of the original model (Rajagopal et al., 2016). BFSH (Fig. 4.2b) is activated in a 20-50% region and could interfere with EMG readings of the actual subject. Thus, the comparison can show a deviation in experimental BFLH muscle activation and simulated BFLH and BFSH. This makes the simulated data for the late stance phase and initial swing phase as false activation, but we expect to see a similar effect due to PAMs. The peaks and their scales do not match for experimental results. The scale for BFLH and ST is different, and the reason is unknown. The comparison is made on the reduced levels of muscle activations.

For BFLH, in Fig. 4.6 ratio actuation is similar to the above simulations where it behaves like PAMs' low actuation. The muscle activations increase before and after the heel strike. For varying actuations of the brace, the reduction in muscle activations can be seen in simulations. The effect is seen clearly for the gait cycle's swing phase (65-90%). The heel-strike event from experiments is faintly matching to the simulations where it leads to an increase in muscle activations for medium actuation.

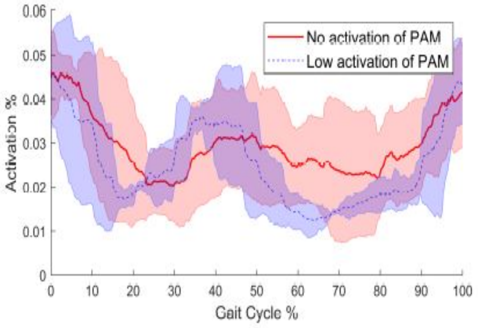

(a) Experimental

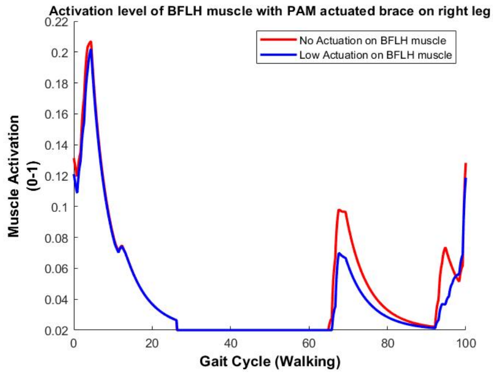

(b) Simulation

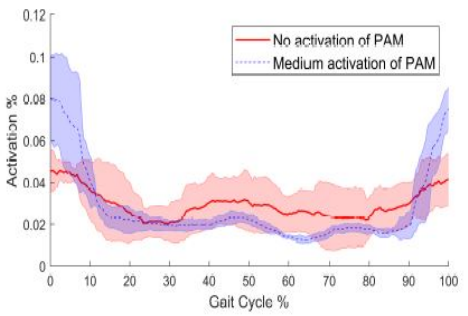

(c) Experimental

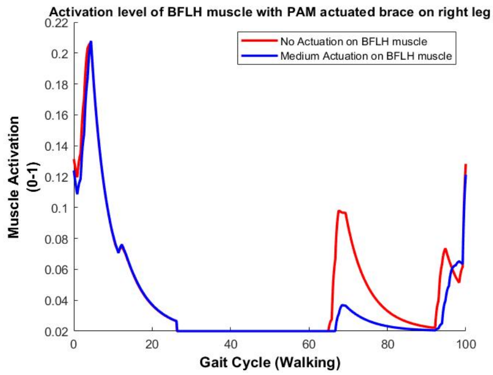

(d) Simulation

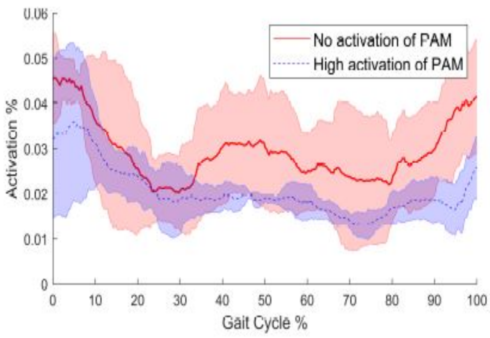

(e) Experimental

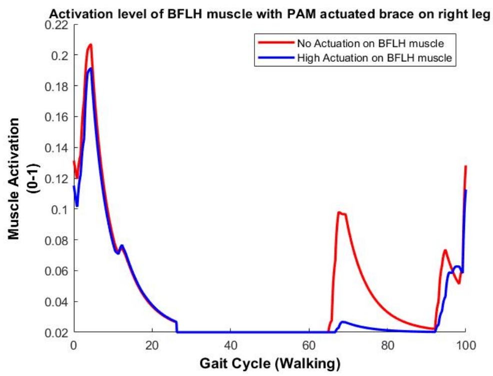

(f) Simulation

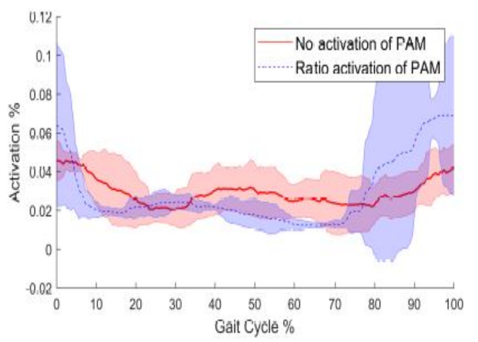

(g) Experimental

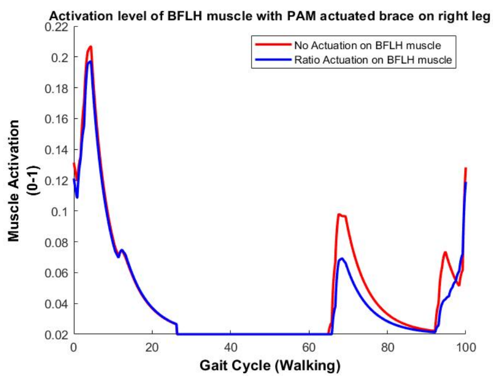

(h) Simulation

Figure 4.6: Comparison of BFLH muscle activations under different PAM actuations. (Parts a, c, e, g are from Khambati, 2019)

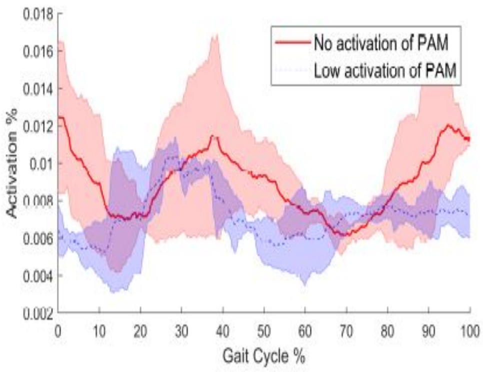

(a) Experimental

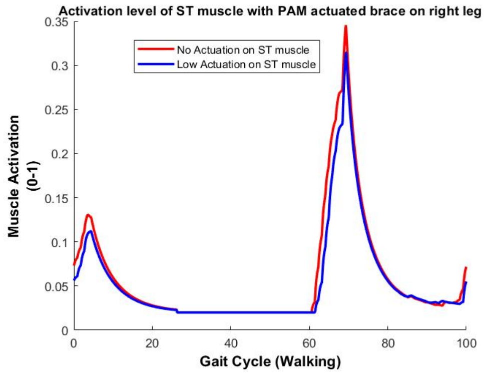

(b) Simulation

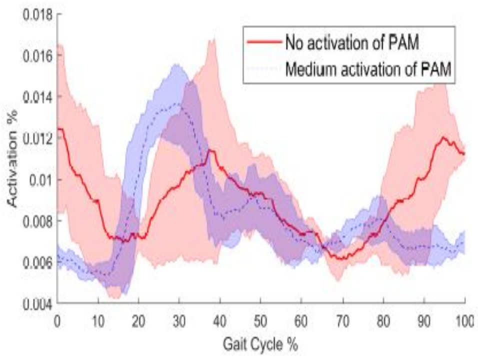

(c) Experimental

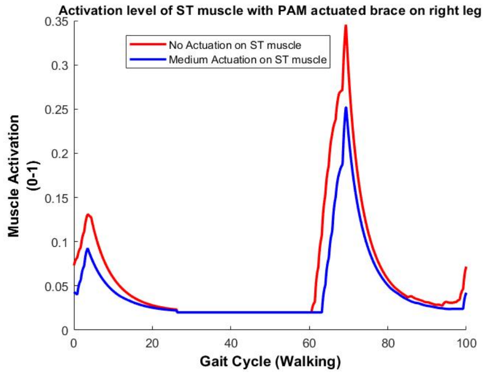

(d) Simulation

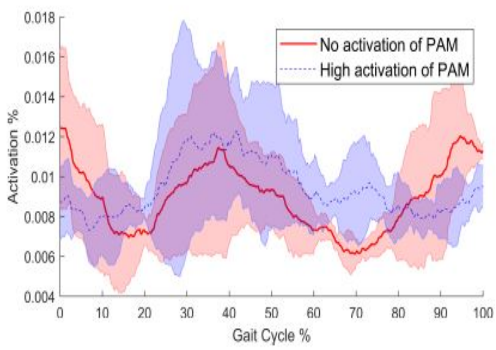

(e) Experimental

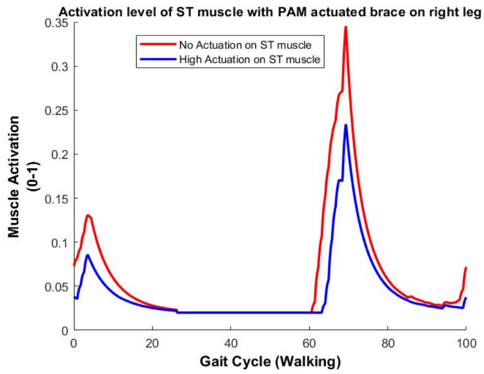

(f) Simulation

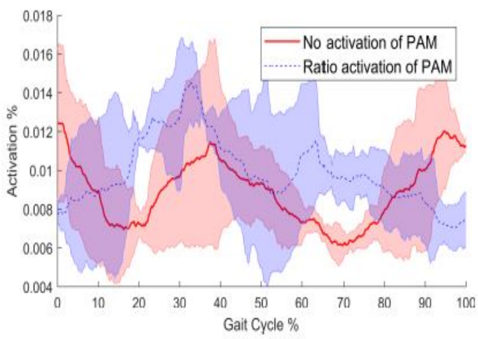

(g) Experimental

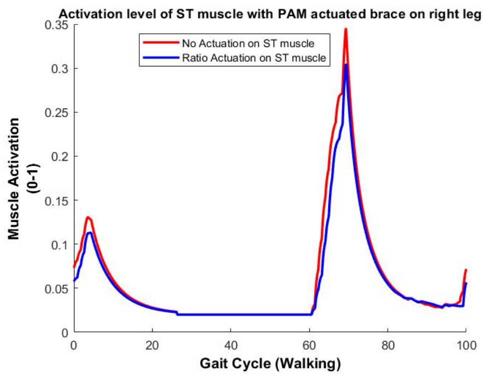

(h) Simulation

Figure 4.7: Comparison of ST muscle activations under different PAM actuations. (Parts a, c, e, g are from Khambati, 2019)

The graphs for ST in Fig. 4.7 are more varied compared to those of BFLH. With increasing actuation forces, muscle activations in ST show a downward trend. But for 20% to 70% of the gait cycle, PAM actuation causes an increase in muscle activity.

The nature of muscle activations in Fig. 4.6 and 4.7 do not match directly in terms of peaks and valleys seen during 30% to 70% of the gait cycle. The difference in experimentally collected muscle activation data and simulated muscle activations is due to the limitations in modeling. These limitations are further discussed in App. C. The simulated results show peaks in muscle activations from 60% to 80% of the gait cycle for both BFLH and ST.

For knee extension, hamstrings act as antagonist's muscles to apply low-level forces compared to quadriceps. During the initiation of motion to allow the limb to start acceleration and gain speed, activation in hamstrings increases. This is also visible when the leg mass needs to be moved against gravity. This is seen from 50% to 75% of the gait cycle and before heel touch. Hamstrings activation decreases as soon the leg starts going in the direction of gravity. This is seen from 10% to 30% of the gait cycle. This shows the swing phase's complexity, where the knee extension with gravity does not exclusively affect hamstrings.

4.4 Different single PAM configurations

The effectiveness of the knee brace in reducing the muscle activations of hamstrings is shown in the previous section. To gain a better understanding of the effect of knee brace on hamstrings, different configurations of PAMs on the knee brace are assessed. Muscle activations of ST and BFLH are checked for four PAM locations on the femur and tibia brace plates. For all the simulations done till now, PAM'A' configuration has been used.

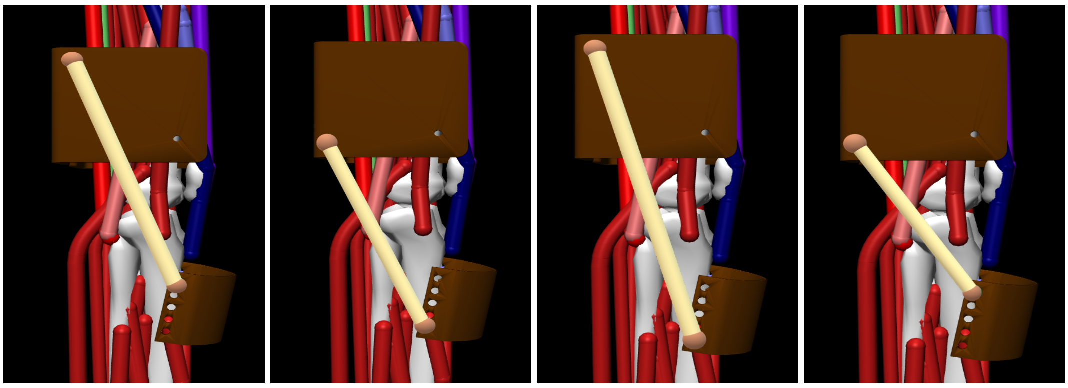

(a) PAM'A' **(b)** PAM'B' **(c)** PAM'C' **(d)** PAM'D'

Figure 4.8: Different single PAM configurations- PAM'A', PAM'B', PAM'C' and PAM'D'

In Fig. 4.8, a lateral view of the right knee with the brace is shown. On the femur plate, the top left and bottom left are chosen for PAM attachments. If the right side of the femur plate is used, the PAMs are much more prone to slack for a large portion of the gait cycle. On the tibia plate, the width doesn't allow much selection except for the top and bottom. The minimum PAM length or maximum contraction without slack is prone to happen in the region where the muscle activity is high. These PAM locations would suggest attachment points of PAMs on the femur and tibia plate for maximum reduction in muscle activations.

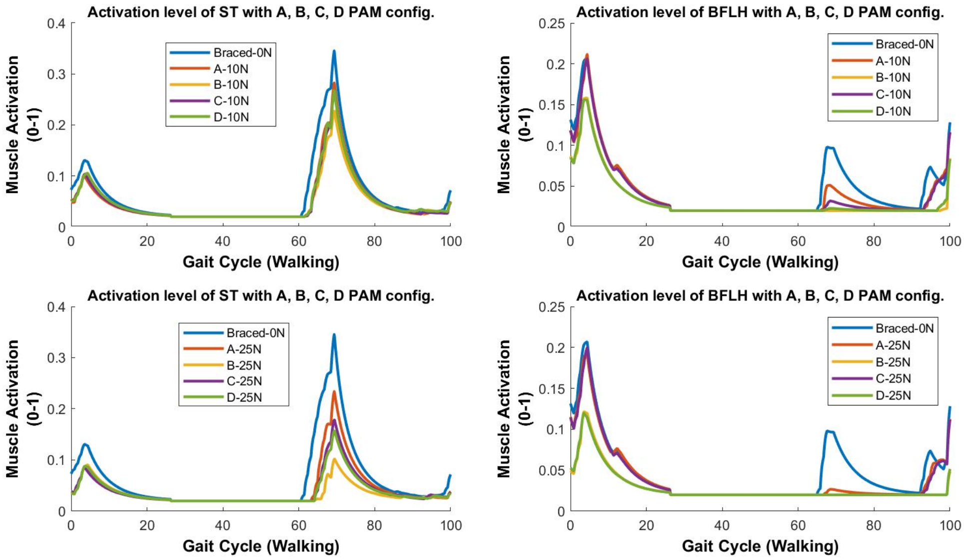

Figure 4.9: PAM'A' vs PAM'B' vs PAM'C' vs PAM'D'

PAM configurations	A	B	C	D
Muscles	Muscle activation levels for 10 N force			
ST	0.28	0.23	0.26	0.27
BFLH	0.09	0.02	0.05	0.03
	Muscle activation levels for 25 N force			
ST	0.23	0.10	0.17	0.15
BFLH	0.03	0.02	0.02	0.02

Table 4.2: Comparison of changes in muscle activation with different PAM configurations

In Fig. 4.9, we can see that for the swing phase from 65-90% of the gait cycle; it is now possible to achieve a 70% reduction in ST muscle activation using PAM'B' configuration at 25 N force actuation. The configuration 'B' has both attachment points at the bottom left of the brace plates. The suggested location of PAM should be on the lower side of both the femur and tibia plate. For ST, PAMs location on both plates is equally important, and the 'B' configuration optimizes both. The BFLH activation during the heel strike event has the same activation of PAM'B' and PAM'D'. For BFLH, the location of PAM on the femur plate is more important than the tibia plate. PAM'B' configuration provides a wide range of activation reduction at different gait phases, making it possible to control knee stability. The activation level differences in the table above show that reduction in muscle activation is ranked as PAM'B'>PAM'D'>PAM'C'>PAM'A'.

4.5 Parallel and Cross Multi PAM (4 and 4x) configurations

Different single PAM configurations on the knee brace and their effect on hamstrings are checked and now two PAMs are attached to each side of the brace. They are actuated so that their combination leads to the specified force (as in single PAM). PAM'4' configuration is a combination of PAM'A' and PAM'B' configurations attached in a parallel. While PAM'4X' configuration is a cross-combination of PAM'C' and PAM'D' configurations, as shown in Fig. 4.10. PAM'4' is prone to physical interactions between PAMs due to their increase in diameter after actuation causing buckling for both PAMs on the side. Thus, PAM'4X' is a hypothetical case as the crossing of 2 PAMs would cause a lot of shear strain and tangle along with the interactions present in PAM'4' configuration.

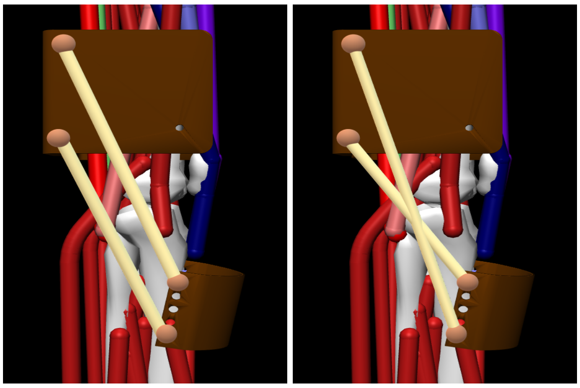

(a) PAM'4' **(b)** PAM'4X'

Figure 4.10: Different double PAM configurations and performance- PAM'4' or Parallel and PAM'4X' or Cross Configuration

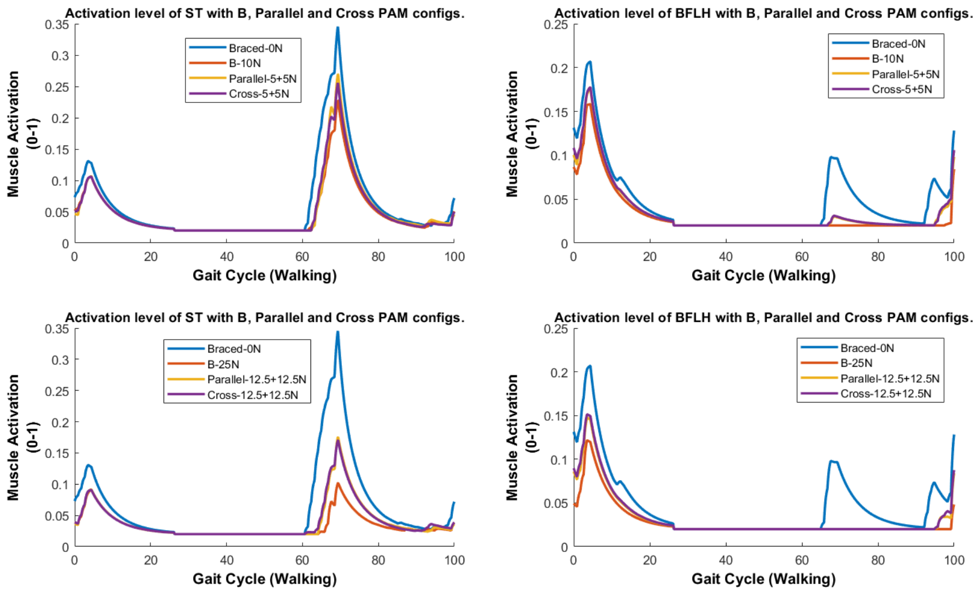

Figure 4.11: ST and BFLH muscle activations for PAM'B' vs PAM'4' vs PAM'4X' actuations

In Fig. 4.11 above, it can be seen that multiple PAM configurations are very close in reductions they achieve. This is due to the combination of one good and one bad PAM location on each femur and tibia plate. They act worse than a single PAM configuration because the best-case scenario in our simulation is two PAMs at or near 'B' configuration, which is essentially PAM'B' configuration.

4.6 Conclusion

In this chapter the model generated in Ch. 3 is used to check the effect caused by PAM actuations on hamstring muscle activations. The model is first simulated to recreate the scenario of self-paced walking with a PAM actuated knee brace attached to the right knee. PAMs on both sides of the knee brace are actuated at different levels of equal and unequal actuation to recreate the experiments performed similarly (Khambati, 2019). The simulation does not show a one-to-one comparison with experiments. The model and simulations need more investigation as they do not collaborate properly with the experiments for all parts of the gait cycle.

However, the simulations show the effectiveness of PAM muscles in taking over the role of hamstring muscles by reducing the muscle activations. The overall reduction in muscle activations using PAM actuation knee brace is corroborated with experiments for the complete gait cycle.

To affect the reduction level in hamstring muscle activations, different configurations of PAMs' on the femur and tibia brace plates are tried. To reduce muscle activations further, the model is tweaked where different locations of PAM attachments are explored and assessed. Now all the simulations were done with PAM'A' configuration. To increase the effectiveness of PAM actuations, four configurations with a single PAM and two configurations of double PAM were checked. All the PAM configurations discussed, whether single or double, can be used to provide varying flexibility in controlling the reductions in muscle activation but PAM'B' configuration is preferred. This is due to the highest reduction in muscle activations for both BFLH and ST in the swing phase and prior to the heel strike event. This configuration will be used further on to check the level of reductions during different phases of the gait for targeted reductions in muscle activations.

5 Controlling Hamstring Activation using Dynamic Actuation of PAMs

With the knowledge of the effects of PAM actuation and its knee brace attachment locations on hamstring muscles, now we will target to control these muscle activations. Till now the PAM actuations were fixed to a value for the complete gait cycle, leading to a continuous PAM actuation to the knee brace and eventually the knee. Now different PAM actuations would be given for different gait phases to provide dynamic actuation.

To control the reduction percentage in muscle activations caused by PAM actuations, we target the reductions in BFLH and ST, individually, with the dynamic actuation of the brace. This would require the knowledge of the motion of the knee to identify the phase it is in during the gait cycle. During walking this knowledge can be attained using neural mapping of muscle activations and knee motion. In our case, these data are available readily without the need for mapping. Simulations also assume instant information transfer of the knee angle for phase detection and ideal force actuation from PAM during the gait cycle. BFLH and ST are being targeted individually, but they cannot be decoupled completely as both are part of the hamstring muscles group. The knee joint model is currently a 1-DoF joint which could be the reason for this coupling.

5.1 Variation in hamstring muscle activations over 0-25 N actuation

The PAM'B' configuration is now simulated with finer force steps of 2.5 N to check for the variations in muscle activations with the PAM actuation for the gait. In Fig. 5.1, we can see large variations in muscle activation levels for both ST and BFLH. These reductions (variations) are not physically viable but important for deductions.

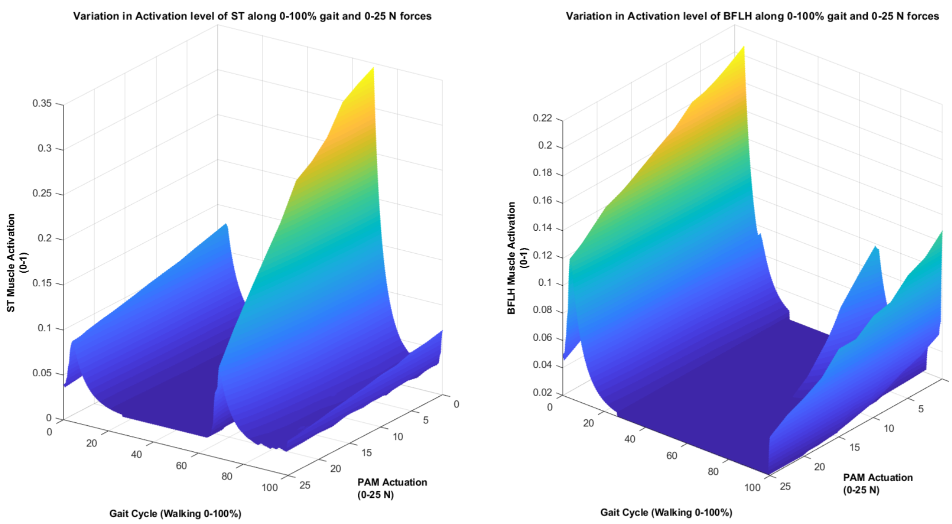

Figure 5.1: Changes in muscle activation levels of ST and BFLH for PAM actuations 0-25 N

Fig. 5.1 shows a 3D plot for ST and BFLH. It contains muscle activations at every point of the gait cycle, with force actuations at 2.5 N step. These values are interpolated for the graph. The slope is continuous for all actuations making it easier to manipulate. ST has such a slope from 65-80% of the gait cycle, while around the heel-strike event, it is saturated. For BFLH, the reduction in activations is more consistent for the heel strike event as compared to ST. Practically, the PAMs' are not able to actuate this fast and this precise yet. However, they can slack, which stops force actuation instantly. A steep reduction in muscle activations is easily possible with higher actuations but is not controllable for the whole gait cycle.

Based on the effects seen in BFLH and ST, a window from 60% to 95% of the gait cycle is chosen where the brace will be actuated with an instantaneous step force profile. The actuation by PAMs for the rest of the gait cycle is kept unactuated to avoid unnecessary extra muscle activation in the antagonist (quadriceps) muscles which are discussed more in App. C.1. For the rest of the gait cycle, either PAM cannot affect hamstrings (early stance phase) or has deficient muscle activation.

5.2 Controlling hamstring muscle activations

With the analysis in Sec. 5.1, we have found the variations in muscle activations of BFLH and ST with PAM actuations over the gait cycle. This supports the usage of PAM'B' configuration in helping to affect hamstring muscle activations effectively (Sec. 4.6). Calculation for the new muscle activity due to the addition of PAM actuated brace is simulated using NMM in Opensim (CMC functionality). The reduction in muscle activations can now be translated to help in supporting the knee of a patient during normal walking.

In Fig. 5.2 the flow of the procedure to be followed for using the model and knee brace is presented. The modeling and simulations used till now are to personalize the model for the patient with ACLd. The target for the knee brace is to reduce ATT motion in the knee due to ACL tear by stabilizing the knee. ATT can be physically measured only through static imaging techniques like MRI/CT. Further, these tests provide the force necessary to reduce ATT at various knee angles. This data when modeled into the NMM is able to recreate and simulate the precise inner working of the knee joint during walking and other motion types. Muscle activations of hamstrings along with knee motion data can be used to map the inputs available from the knee brace to identify different phases of the gait cycle. sEMG, knee angle (potentiometer), and neural mapping can be used to achieve the targeted muscle activations.

This goal requires PAM actuations to mimic and take over a hamstrings muscle group (Sec. 1.3). In ACLd patients, an increase in quadriceps muscle activations and thereby force leads to increased ATT. Increased hamstrings co-activation is required to stabilize the knee joint. This takes time as is done usually through rehabilitation. If the PAM actuated knee brace is used then it can complement the hamstrings directly throughout the rehabilitation procedure leading to stabilized knee and normal gait even with the injury.

For a healthy subject, it means reducing hamstring muscle activations with PAM actuations. This can be achieved by enforcing kinematics and dynamics, of brace model (Sec. 3.4), on simulations of a walking healthy patient's NMM (Sec. 2.5.2). Enforcing a PAM actuation on a healthy knee reduces the muscle activations of BFLH and ST in experiments (Sec. 2.4) and simulations (Sec. 4.3). Continuous PAM actuation has shown to affect heel-strike event and swing phase in gait cycle for these muscles (Fig. 5.1). To reduce the extra load on hamstring muscles due to continuous PAM actuations, dynamic actuation of PAM is done.

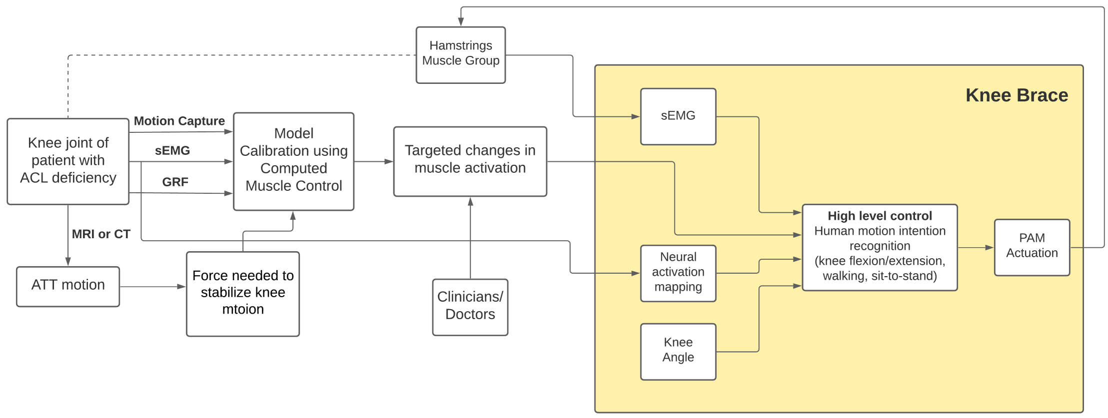

Figure 5.2: Full flow

PAM actuations have been constant throughout the gait cycle (Ch. 4). Two targets of 20% and 50% reduction in hamstring muscle activations are checked and then simulated using dynamic actuation. PAM's dynamic actuation has a 0.25 N step for a 0.012 s time step (or 0.01% gait cycle) for further simulations. CMC function is used with prescribed PAM actuations based on the knee angle for further simulations.

To use the dynamic actuation of PAM, we checked the effects of continuous PAM actuations on BFLH and ST. From Fig. 5.1 we can see that controlling ST and BFLH for the whole gait cycle period is not possible. Hence, we would now focus on reducing the hamstring muscle activations by 20% and 50% (with respect to 0 N actuation) for the full gait cycle. Fig. 5.3 and 5.4 shows the PAM actuations required for targeted reduction in muscle activations in ST and BFLH. Fig. 5.3 shows that certain periods of gait have a fixed reduction in ST activation. This happens during 85-100% of the gait cycle of ST, for the 20% reduction target. When this is compared to the 50% reduction target, we see that we lose control over a wider range of the gait cycle. These periods of gait cycle saturate in their possible reduction levels. The peaks at 27% and 63% of the gait cycle are discontinuous. This is due to the sudden changes in PAM actuations at events with changing ground contact dynamics.

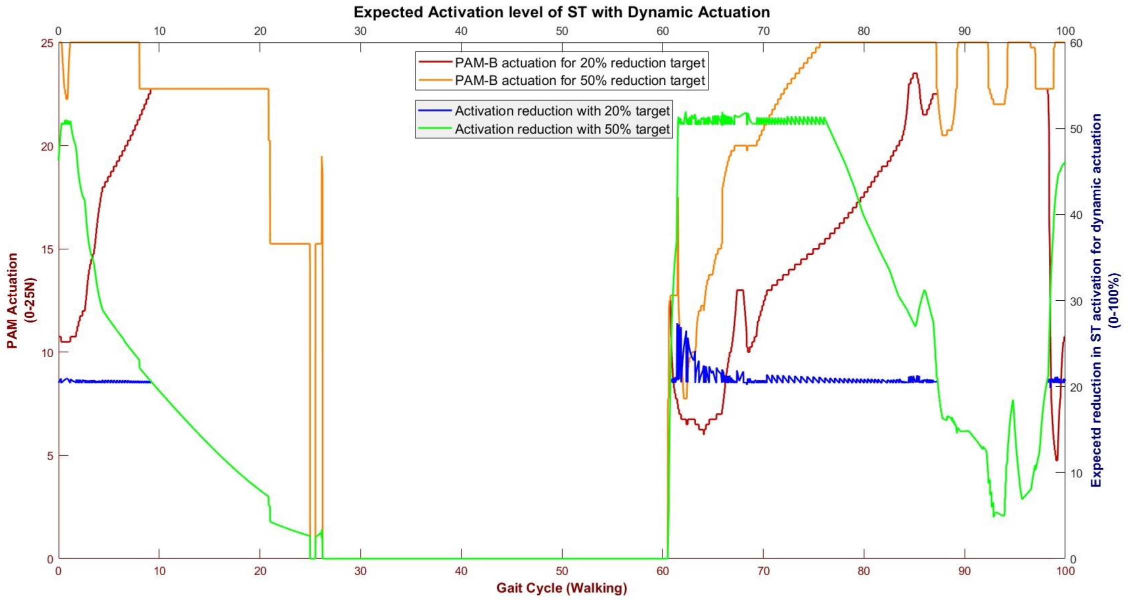

Figure 5.3: Expected ST muscle activation with dynamic actuation of PAMs for targets of 20% and 50% reduction in muscle activation

Comparing Fig. 5.3 and 5.4, we see that the expected reduction at 20% target is more consistent for BFLH when compared to ST. Fig. 5.4 shows that certain periods of gait cycle have a fixed reduction in BFLH as well as ST. This happens during 85-95% of the gait cycle of BFLH for both 20% and 50% reduction targets. For the 50% reduction target in ST muscle, we see that we lose control over a wider range of gait cycles, which is at 5-25% and 75-95%, due to saturation in reductions. There are two steep peaks at 68% and 93% of the gait cycle in the muscle activation reduction of BFLH in Fig. 5.4.

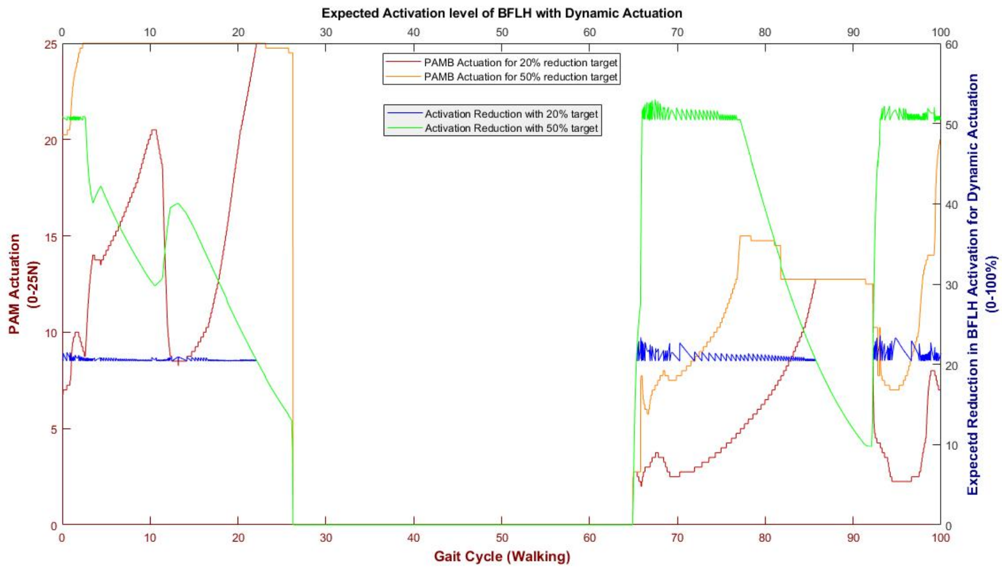

Figure 5.4: Expected BFLH muscle activation with dynamic actuation of PAMs for targets of 20% and 50% reduction in muscle activation

On comparing the possible effects of dynamic actuation on BFLH and ST, we found BFLH to have a wider range of effects. During the gait cycle for the swing phase and heel strike event, there are regions where a lot of muscle activation reduction can be made. From here on, we would focus on controlling BFLH muscle activation.

5.3 Targeted reduction in hamstring muscle activations

The simulations are done for 20% and 50% target reductions in BFLH muscle activation using dynamic PAM actuation. The results, as shown above in Fig. 5.5 do not match the expectation. The target reduction of 20% causes an increase in muscle activation. The 50% target reduction at this point should reduce muscle activation as it is for 25 N actuation. A similar effect is seen in the swing phase, where the reduction is not as expected.

Upon investigation, it was seen that if the targeted actuation's for the PAMs are this steep and sudden, then OpenSim would produce incorrect results. The forces should be present before the actual motion happens to support the muscles at peak activations. Thus, the peak at 63% needs actuation from 60% of the gait cycle. This is tested and found to match the expected response.

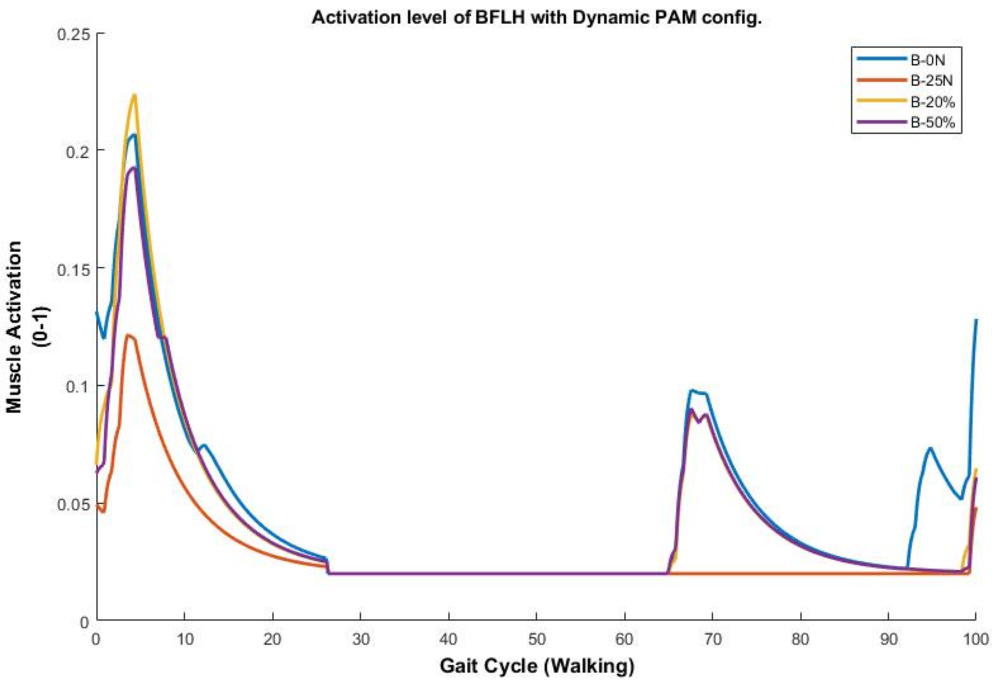

Figure 5.5: Simulated BFLH muscle activation with dynamic actuation of PAMs for targets of 20% and 50% reduction in muscle activation. 0 N and 25 N continuous PAM actuation for reference as minimum and maximum reduction possible.

When CMC simulation is done, it takes into consideration the whole data profile for optimization. It has a Proportional Derivative (PD) controller to meet muscle activations for the desired output. It calculates the optimized activation levels at each timestamp to avoid sudden impractical muscle responses.

Such responses happen during changes in contact with the ground (or external forces). Averaging out of the response is needed to impact the peaks of muscle activation properly. This results in some gait periods being averaged out, leading to a 10-18% increase in muscle activation reduction from the targeted reduction percentage.

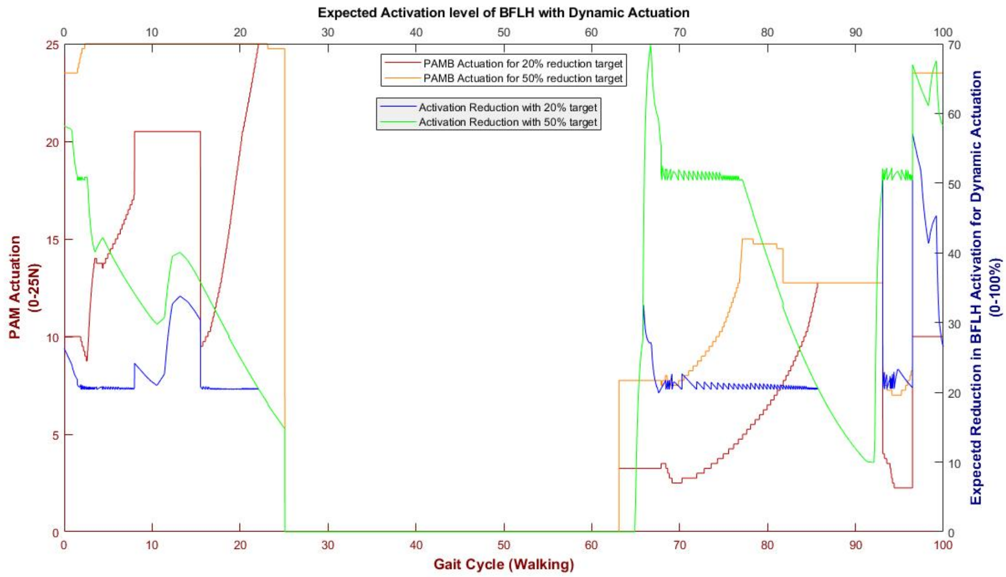

Figure 5.6: Expected BFLH muscle activation with modified dynamic actuation of PAMs for targets of 20% and 50% reduction in muscle activation

Fig. 5.6 shows the corrected PAM actuations, and it's corresponding expected muscle activation levels. This is done by starting the required PAM actuations before the actual point of need. Due to this averaging, the actual reduction varies from target causing loss of control. With increasing levels of reduction percentage required, we lose control over the gait phase due to saturation of effect of PAMs on muscles. There is still a discontinuity at 97% gait cycle, which should have been smoothed out but is not as it would lead to complete loss of control for BFLH activation.

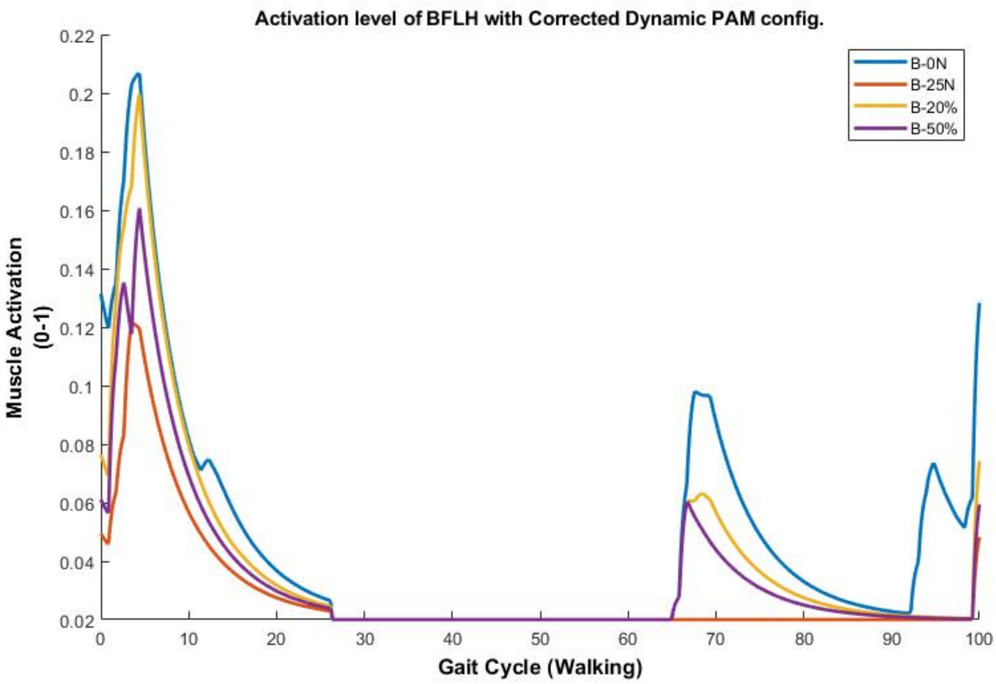

Figure 5.7: Simulated BFLH muscle activation with modified dynamic actuation of PAMs for targets of 20% and 50% reduction in muscle activation. 0 N and 25 N continuous PAM actuation for reference as minimum and maximum reduction possible.

Fig. 5.7 shows the simulated results for the corrected dynamic actuation. The reduction effect has increased significantly compared to the previous input. For the initial gait cycle, the peaks do not provide a sufficient and consistent decrease in activation. In this range, the 50% reduction target is actually able to provide a 20% reduction in muscle activation. This shows the effect of the PD controller used in CMC for overall gait. The reductions in the swing phase are not near the target. The swing phase variations could be due to shifting the peak with higher PAM actuations leading to a higher peak to peak difference.

The hamstring muscle activations can be reduced using continuous PAM actuations but not with dynamic PAM actuations. This happens due to the PD controller embedded in the CMC function (3.5.3). The PD feedback allows to follow the prescribed trajectory after SO and FD steps. The feedback loop calculates for every 0.01 s time step while the chosen PAM actuations are considered much faster. Averaging the PAM actuations defeats the purpose of dynamic actuation as it leads to the requirement of higher and continuous PAM actuations. Dynamic actuations are not preferred for simulations currently.

5.4 Conclusion

For most of the simulations and comparisons done in Ch. 4, continuous actuation of PAMs has been used for the entire gait cycle. In this chapter dynamic actuation of PAMs is explored. Here the PAMs are actuated based on the different phases of the gait cycle. This is done to reduce the PAM actuations for the phases of the gait cycle where the muscle activations are too low or unaffected. This would avoid muscle activations in antagonistic quadriceps muscles. The continuous force actuation of PAM is a more realistic option when PAM actuation speeds are taken into consideration. There are important points in the gait cycle that affect the muscles for longer periods even after the motion. This is due to their tendency to expand slowly as compared to contraction. To vary the muscle activations of individual muscles using PAM, a more detailed model and further experiments are needed.

6 Conclusion

A neuro-musculoskeletal rigid body model (Ch. 3) has been used to simulate muscle activations in knee joint during walking gait (Rajagopal et al., 2016). Generating such a model requires data from sensors (App. A) through experiments. Motion capture, GRF and EMG provide a framework for sensor data fusion, which provide data for kinematics, dynamics and neural excitation, respectively. Opensim is used to modify the model to add the PAM actuated knee brace to right knee joint and simulate.

PAM brace model (Ch. 4) consists of 2 brace plates attached to the femur posteriorly and tibia anteriorly. The actuator are simulated as point actuators acting force along the PAM length axes. In the simulations, the model is forced to follow the same kinematics and dynamics of the walking gait with PAM brace around the knee. This leads to PAMs complimenting the hamstring muscles for the motion of the knee joint. The brace when actuated for the gait cycle, is able to produce reduction in muscle activations of ST and BFLH in healthy subjects as reported in earlier experiments (Khambati, 2019). Simulations done are in agreement to the results presented after the experiments. The PAM actuated brace is able to reduce the muscle activations in BFLH and ST muscles. The reduction is not apparent for some gait phases but reduction is visible when the complete gait cycle is considered.

To increase the reduction in muscle activations, different PAM configurations (Ch. 4) are explored. PAM'B' configuration is selected due to the increased reduction in hamstring muscle activations after heel strike event (which occurs at the starting of the gait cycle). Configuration with multiple PAMs on either side of the knee brace is simulated but found to produce no substantial difference when compared to PAM'B' configuration.

The PAMs were given a constant actuation for the whole gait cycle in all the simulations done till now. With dynamic actuation (Ch. 5) of PAM it is possible to modify hamstring muscle activations as per the requirement of reduction in muscle activations needed. ST and BFLH muscles are checked for 20% and 50% target reduction in muscle activations. The controllable periods in these muscles are near the heel strike event and swing phase. BFLH shows more phases of the gait cycle where the reduction in muscle activations do not saturate when a 50% target reduction is given. The expected targets are not met when simulated. The effects of changes in contact forces is seen to propagate through next phases due to the PD controller being used internally for CMC simulation. This makes the targeted reductions in muscle activation difficult to achieve. Continuous activation of PAM is more suited in a practical way as fast actuations are currently not possible.

The model and its simulations provide an initial framework to simulate the knee joint for ACLd patients. Currently, reduction in muscle activations are targeted in healthy subjects to check the effectiveness of the PAM actuated brace in complimenting hamstrings. This will help ACLd patients to use PAMs as support for hamstrings to stabilize knee during daily living activities.

6.1 Model Limitations

- Current model has no component to simulate ligaments (ACL) and is a 1 DoF knee angle coupled joint. Currently, ATT motion is coupled to knee angle.

- PAM is a set of point actuators with their mass focused on the attachment clamps at both the femur and the tibia plates. No wrapping of PAM around brace or knee is modeled. Skin to brace shear strain and slippage are also not modeled.

- The femur and tibia brace plates are not interconnected but separately attached rigidly to the femur and tibia bone respectively.

- CMC residual actuators should not be more than 25N. Residual actuators had limit of 10-15 N which was crossed as PAM actuation increased (App. C.1). This is expected as quadriceps activation increases during such actuations. Increased quadriceps muscle activation is an undesired effect.

6.2 Future recommendations

To further the research following steps are suggested with the current model:

- The model to include ligaments to simulate the effects of ACL deficiency properly. ATT and Internal-External motion needs to be modeled to improve the study regarding with effect of PAMs on hamstring muscle activations.
- Experiments are required with EMG, motion capture and GRF for braced and non braced conditions to check for the effect of PAMs as a co-actuator to hamstring muscles. Affect on quadriceps muscle activations due to the PAM actuations also needs to be explored.
- Co-simulation- Opensim is used to calculate kinematics, dynamics and neural activations of a macro NMM focusing on lower extremity for large motions. This is further complimented with a detailed Finite Element micro model for the loading and movement of ligaments and meniscus. This combination can be used for optimizing the neural activations with inclusion of ATT (Esrafilian et al., 2020).
- EMG assisted model with hamstrings and quadriceps muscle activation data can be a better model for checking the effect of PAM actuations.

Appendices

A Sensors and Actuators

To check knee health, a descriptive measurement of knee behavior is needed. This requires sensors to measure the motion of the knee joint and forces generated by muscles. To manipulate muscle activations of the knee, an actuator based knee brace is needed. To measure the effectiveness of such a brace, sensors are needed to collect data for investigation. Such sensors and actuators are discussed in this chapter.

When supported with PAM actuators, sensors provide a knee brace that will be able to co-activate with hamstrings. Computer models can be useful tools for a more detailed understanding of the dynamic interactions between muscles, bones, and ligaments. With the data collected from sensors, we can recreate the internal body workings.

To assess the brake actuation system's effectiveness on knee muscle behavior, we need measurements of neural muscle activations, kinematics of human motion, and force data for reference in a model. Simulations require experimental data on:

- Marker trajectories or joint angles from motion capture
- Force data typically ground reaction forces and moments and/or centers of pressure
- surface Electromyography (sEMG)

A.1 Motion data

Motion data involves the measurement of physical parameters related to kinematics. This includes linear and angular kinematics of different body parts to inverse the body's kinematics properly.

A.1.1 Potentiometer

A potentiometer is used as a goniometer to measure the range of motion of a rotary joint. It is used to calculate knee flexion angle on both sides of the knee. This allows the calculation of internal-external rotation during walking. This is used with a gear mechanism to allow rotation and to measure the knee angle accurately. The hardware is shown in Fig. A.1. It is used as the sensory input in knee brace (Khambati, 2019).

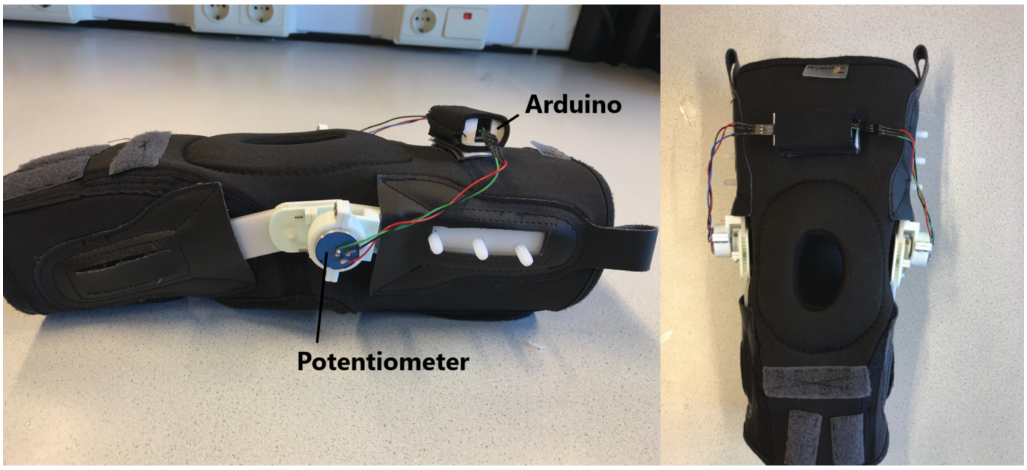

Figure A.1: Potentiometer integrated in the rotational knee joint connecting femur and tibia side supports. Data acquisition of both potentiometers is done using Arduino Uno micro-controller. (Khambati, 2019)

A.1.2 Inertial Measurement Unit (IMU)

IMU works by detecting linear and angular acceleration, using accelerometers and gyroscopes, respectively. This is used to calculate the velocity and position of the mounting location. It is commonly used for navigation purposes in UAVs, ships, etc. Low-cost IMUs are used for detecting orientation and motion in smartphones, gaming devices, sports, animation, and medical devices. This provides the kinematics data of the motion.

IMU has the disadvantage of accumulating error if their reference is not corrected frequently. This error increases with an increasing period of inactivity (no acceleration). To detect knee motion, sensors should be placed at points with a higher range of motion. This is important to measure proper motion and avoid the integration bias error due to inactivity. IMUs mounting on non-rigid surfaces like the skin is proven to be difficult due to slippage.

A.1.3 Visual Markers

Visual Markers is a motion capture technique using an arrangement of visual cameras surrounding a subject wearing markers. These markers, when tracked, generate motion data. Marker types vary from spherical balls to Quick Response (QR) codes. Using visual markers requires a space-constrained permanent setup for accurate data acquisition and high-level post-processing of visual data.

They require a similar placement technique as IMUs but with an added requirement of having at least 3 non-colinear markers for triangulation. Using visual markers is less accurate than IMU sensors but compensates this deficiency by adding more markers as markers are cheaper than IMUs. Visual markers are generally used along with IMUs for better coverage of superficial kinematics (Fig. A.2). These differences make Visual Markers good for modeling and calibration, and IMUs for real-time applications.

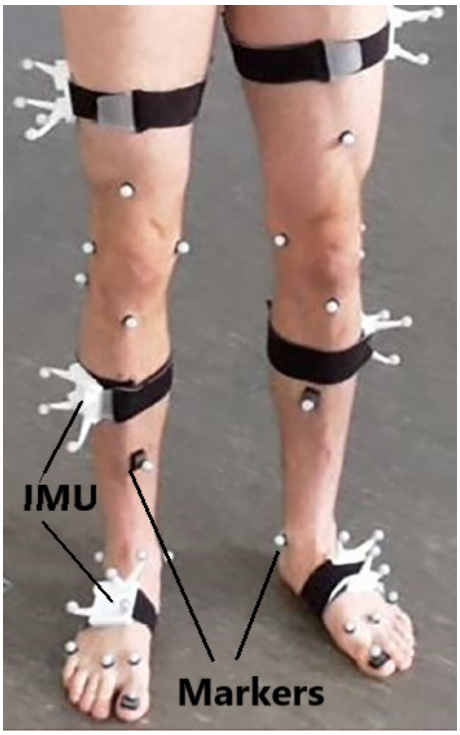

Figure A.2: Visual Markers and IMUs are attached to skin using adhesive and straps, respectively. (Teufl et al., 2019)

A.2 Ground Reaction Force (GRF)

Force transducers like load cells are used as force plates to calculate forces exerted during walking, standing, jumping, etc. 1-Dof force plates can only calculate the vertical component of force at the center of pressure. In contrast, 3-Dof plates can calculate shear forces, vertical forces, and moments. Motion data (kinematics) with force information of load-bearing in different axis is calculated as shown in Fig. A.3. Dynamic force loading along with kinematics and muscle activations provide a complete set of data required to simulate the interaction between muscles, bones, ligaments, etc. This is calculated using a setup shown in Fig. A.3 where the subject walks on the plate.

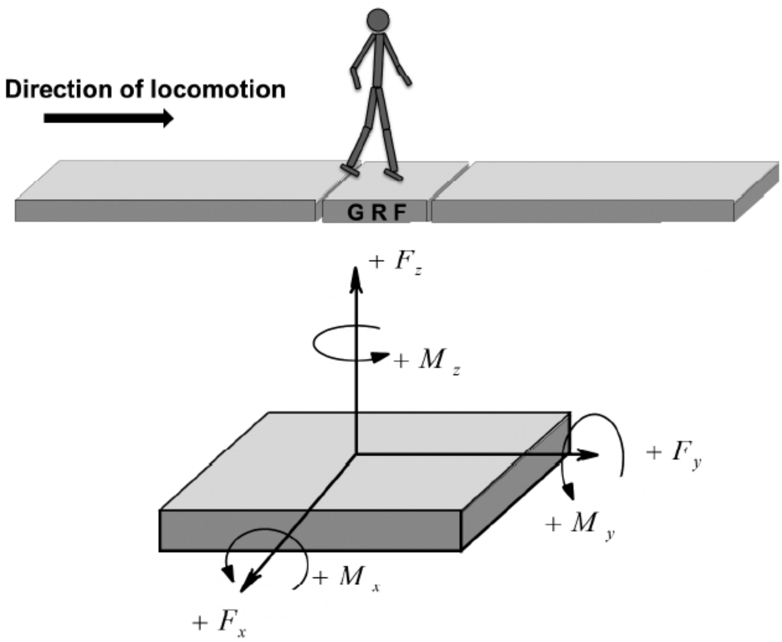

Figure A.3: Forces and Moments are calculated by Ground Reaction Plates when walking over it. Forces and moments in all directions are depicted. (Eguchi et al., 2016)

B Anterior Cruciate Ligament deficiency (ACLd) and tests

ACL is one of the four main ligaments attaching the femur and tibia. Others are posterior cruciate, medial and lateral collateral ligaments, helping to stabilize the knee by providing restraints to the knee's motion, shown in Fig. 2.6a. Contact injury is a common reason for an ACL tear is also accompanied by other ailments of the joint. Certain abrupt motions of the knee joint not involving any impact can also cause ACLd.

ACL reconstruction (ACLr) is a surgical option where a graft is taken from the hamstring muscle or quadriceps to reinforce the ruptured ACL. It does not restore the knee to its prior injury state. Such effects are discussed in the next section.

Loss of constraints due to ACLd produces unwanted motion between femur and tibia on anterior-posterior axes. This motion is known as Anterior Tibial Translation (ATT), the relative motion of tibia bone (near patella) with respect to the femur during knee flexion. ATT is not the only constraint lost after ACLd; internal-external rotation of proximal tibia is also increased with respect to the femur. Knee extensor torque increases, causing instability. The increased knee torques and contribution of muscles during high flexion angles (>60°) varies highly (Shelburne and Pandy, 2002) patient to patient.

To check such deficiencies, multi-directional laxity tests (Fig. B.1) are done to measure different mechanical properties of soft tissues like ligaments (Nicolella et al., 2011). In clinics, there are some tests for checking ACLd as presented following.

B.1 Drawer and Lachman Test

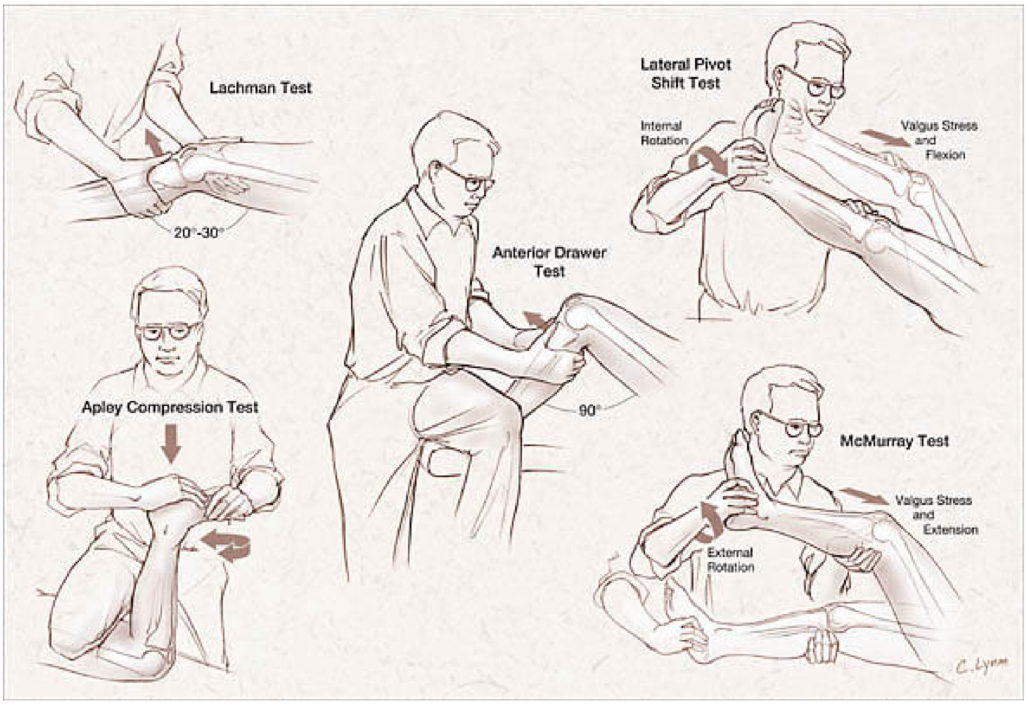

Figure B.1: Different Laxity Tests checking variations during specific motion. (Solomon et al., 2001)

The Lachman test is a passive accessory movement test of the knee performed to identify the ACL's integrity. Other tests are also used to check knee stability by checking the varus-valgus stress and internal-external rotation. A clinical examiner does this test to check for translation. Although the Lachman test is superior in checking tear in ACL than the Anterior Drawer test, it cannot give the exact ATT calculation. Increased co-activation of hamstring muscles is also a reliable source for ATT detection (but not for its measurement). A Pneumatic Lachman setup is used to measure ATT and other Ligament details, which is compatible with Magnetic Resonance Imaging.

B.2 X-Ray Computed Tomography (CT) and Magnetic Resonance Imaging (MRI)

X-rays are used to detect bone fractures and muscle tears. Ligaments have density 1000 times lesser than bones, making them a soft tissue that is not detectable with X-rays.

As a superior method, a CT scan is used to detect hairline or subtle fractures and ligament tears by creating a 3D map of the knee. While being widely available, both methods are not suggested for rehabilitation due to high doses of radiation.

To avoid all these drawbacks, MRI is used. It uses magnetic field and radio signals to create a detailed (more than CT) 3D image with bones, muscles, and soft tissues. It is used to obtain detailed measurements of different motions across the knee joint. It also provides details about ligament extension and meniscus distribution. It can be used frequently as it is also free from ionizing radiation. CT and MRI tests are costly and take long periods of measurement. Thus, they are used mainly for detecting ligament tears or damage to the meniscus.

In Lachman, MRI, and CT tests, we measure only at the knee joint's static poses. The dynamic effect of force interaction during various motions is limited. It is calculated using knee cadavers (Naghibi et al., 2020). Cadaver based experiments have been done by medical personnel to identify different muscle, bone, ligament, neural interactions, and physical properties. In many studies, cadaveric experiments involved restricting muscle groups so that only a particular set is being used. This makes the experiment focused and only reliable in isolated conditions (Ali et al., 2017). Surgical implants utilizing a large array of sensors inside the cadaver for detailed data acquisition (Naghibi et al., 2020) during different knee motion. These techniques, combined with other sensors (Sec. 2.2), help identify different effects of ACLd on various components of the knee joint.

C Opensim Model

Opensim v4.1 is standalone software with GUI, C++, Python and Matlab functionalities. Simbody is the physics engine for multibody dynamics. It uses Featherstone-style formulation of rigid body mechanics to provide results in reduced order from n^3 to n time for any set of n generalized coordinates with arbitrary constraints.

Opensim has changed vastly from v3.3 to v4.1. Thus latter is suggested for modelling and simulations. Changes to models are made in the ".osim" (xml) files in text editor. Matlab (R2018b) and Opensim GUI are capable of simulating all functionality of the software, sequentially. Due to the linear structure of interpreted compilers, multiple instances of simulations are not possible in GUI, python or Matlab. Thus, a code for multiple simulations is developed in Microsoft Visual Studio Community 2017 to save time and effort.

Removal of internal-external rotation in the knee joint model causes transfer of motion from the femur to hip joint (McLean et al., 2003). This leads to the mass of the femur being added to the rotational inertia of the tibia. This could lead to large deviations from 25N (App. C.1). RRA can produce large variations from IK data measured using sensors. GRF data is critical for RRA analysis.

We are also enforcing a new dynamic structure on a previously optimized model. This is bound to create abnormalities. Residual Reduction Analysis (RRA) is another opensim functionality not discussed in Ch. 3. It is used to complement IK and Model using the 17 torso actuators for increasing dynamic consistency with GRF data. Residuals are expected to be within the 25 N range. Simulations showed that this was not the case.

Fig. C.1 shows the muscle activation of BFLH muscle as measured (Rajagopal et al., 2016) and simulated (Rajagopal et al., 2016). The experimental (Khambati, 2019) and simulated (Ch. 4) show similar changes in muscle activations. The effect of PAM actuations on ST and BFLH are compared for the reductions in muscle activations caused for the gait cycle on whole.

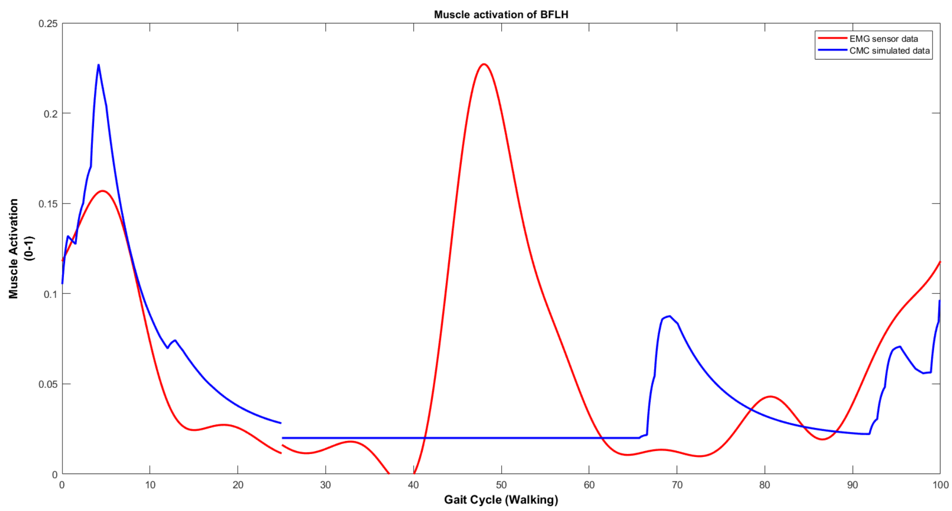

Figure C.1: Comparison of experimental data and CMC simulated data (Both from Rajagopal et al., 2016). The data collection started from 25% of gait and thus has a discontinuity at that point

C.1 Quadriceps

Hamstring facilitation vs quadriceps avoidance (probably to reduce anterior shear) for ACLd patients to reduce ATT during walking. Reduction in knee extensor moment by decreasing quadriceps muscle activation. But not enough to get to intact knee level even after muscle activation reduced to zero (Berchuck, 1990). It has been shown that increasing the hamstring co-activation helps in restoring ATT (Liu and M. E. Maitland, 2000). Simulations showed that increased hamstring muscle forces produced an additional knee flexion moment that must be balanced by a corresponding increase in a quadriceps muscle force. Thus we focused more on supporting the hamstring than reducing forces in the quadriceps.

With PAM actuation we achieved higher quadriceps forces which could affect knee stability adversely like inefficient motion requiring higher energy consumption. Simulations show quadriceps and hamstrings muscle forces increase with increasing knee flexion angle while studies show 15-20°as most crucial for ACLd patients. The quadriceps muscles develop higher forces than the hamstrings at all flexion angles above greater than 20°(Shelburne et al., 2005b). But, during walking gait, high ACL load is seen at flexion angles less than 10°. This shows that the increase in quadriceps muscle activation will not impact ATT stability during the stance phase (Shelburne and Pandy, 2002). The increase in quadriceps muscle activation is due to the reduction in hamstring muscle activation. As they are a pair of antagonist and agonist muscles this is expected. Strain in the ACL can be minimized by exercises or activities that co-activated the quadriceps and hamstrings in knee flexion angles greater than about 30 degrees and demand low force from the quadriceps, regardless of knee angle.

Simulations showed that increased hamstring muscle forces produced an additional knee flexion moment that must be balanced by a corresponding increase in a quadriceps muscle force.

Increased co-contraction of antagonistic muscles would decrease motion efficiency, and increase energy expenditure and tibiofemoral contact force.

In chronic ACL-deficient knees showed an adapted gait pattern to avoid peak quadriceps muscle force (Berchuck et al., 1990; Andriacchi, 1993).

C.2 Graphs for hamstrings, quadriceps, and residual actuators

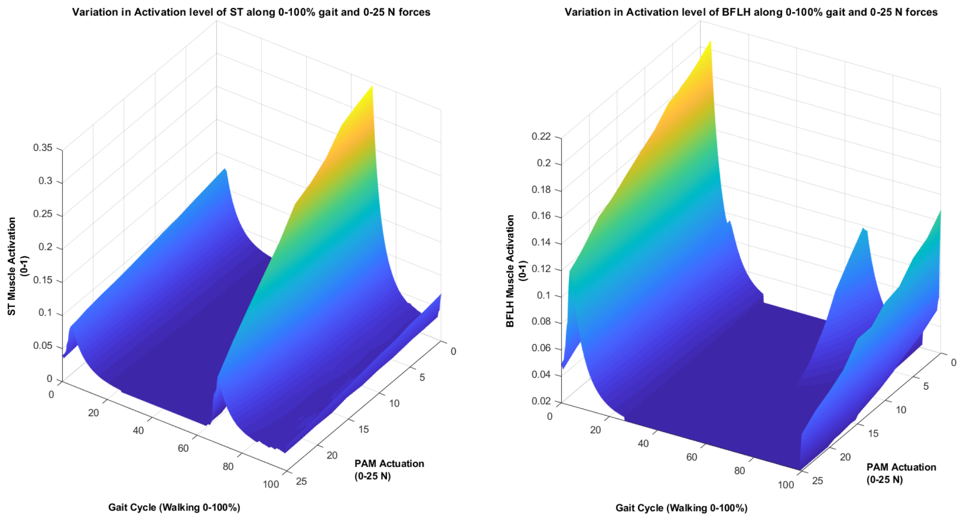

Figure C.2: Changes in muscle activation levels of ST and BFLH for PAM actuations 0-25 N. Same as shown in Ch. 5

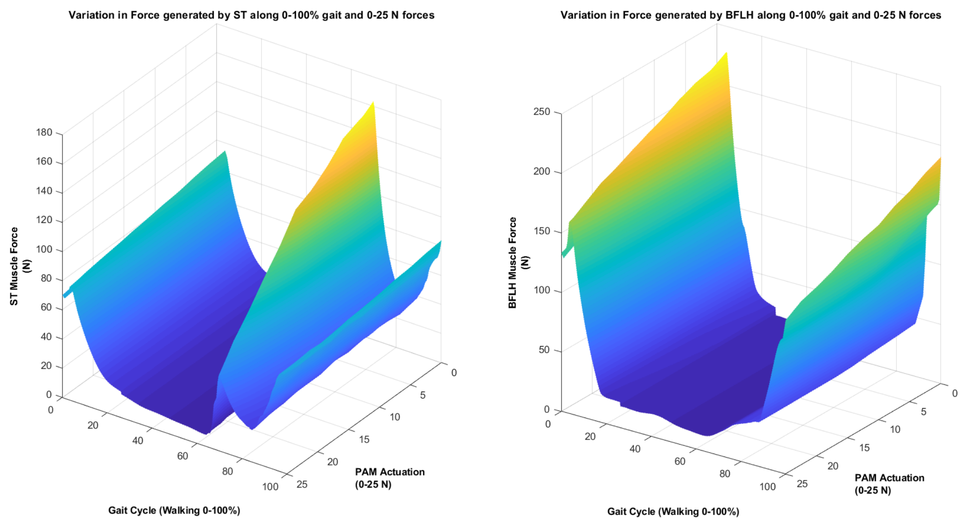

Figure C.3: Changes in force generated by ST and BFLH for PAM actuations 0-25 N

Fig. C.2 and C.3 show the muscle activations and forces generated in the muscles ST and BFLH using CMC simulations of the model. The forces generated and muscle activations can vary due to the passive forces generated in the muscles due to constraints provided by the motion of other muscles and bone structures.

Similar figures are presented for the muscles SemiMembranosus (SM) and Biceps Femoris Short Head (BFSH) in Fig. C.4 and C.5. Vastus Lateralis (VL) and Vastus Medialis (VM) in the Fig. C.6 and C.7. Vastus Intermedius (VI) and rectus femoris (RF) in Fig. C.8 and C.9.

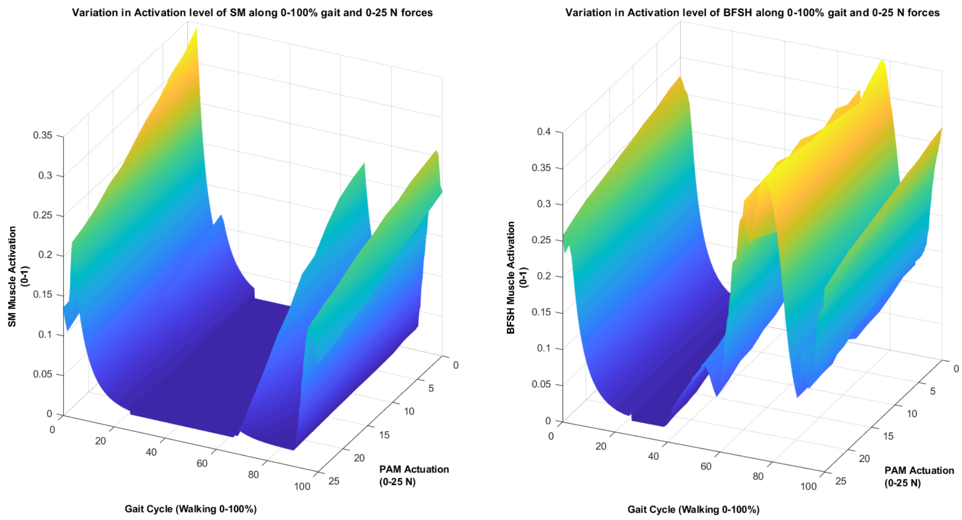

Figure C.4: Changes in muscle activation levels of SM and BFSH for PAM actuations 0-25 N

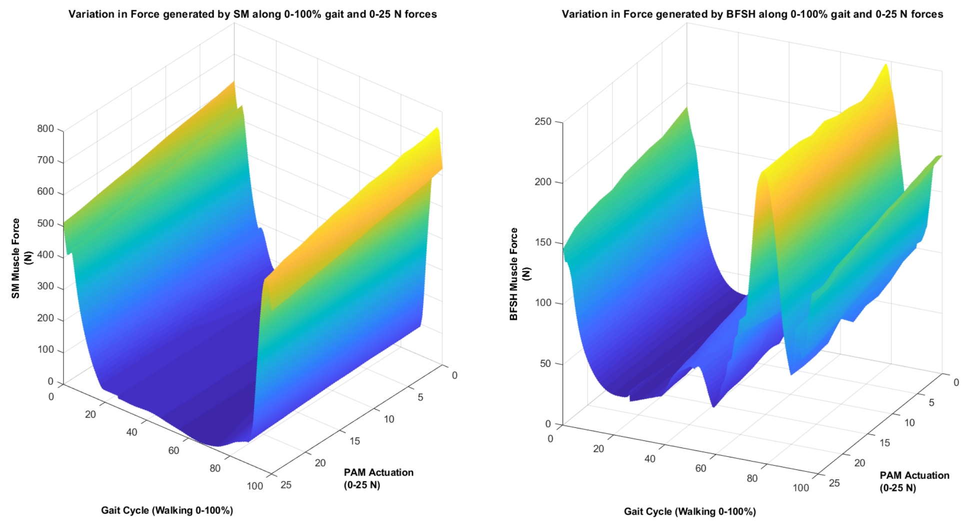

Figure C.5: Changes in force generated by SM and BFSH for PAM actuations 0-25 N

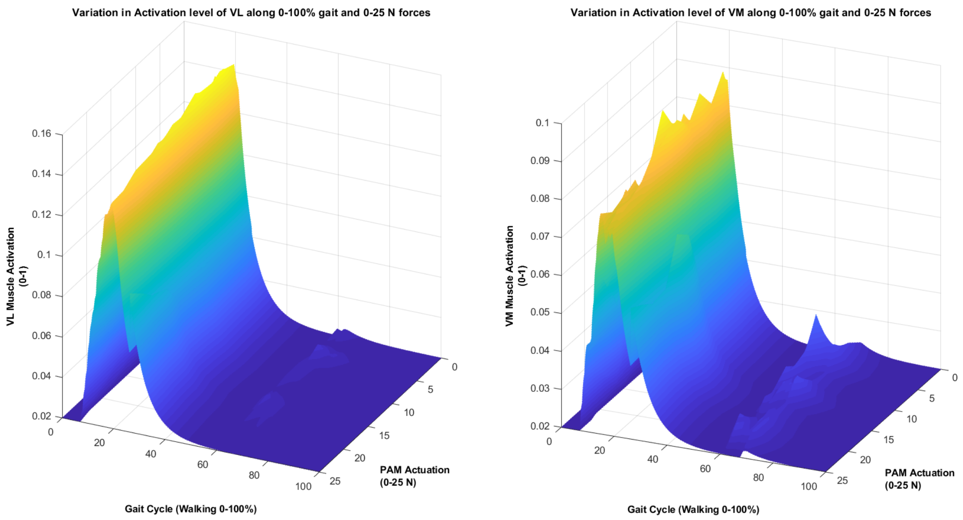

Figure C.6: Changes in muscle activation levels of VL and VM for PAM actuations 0-25 N

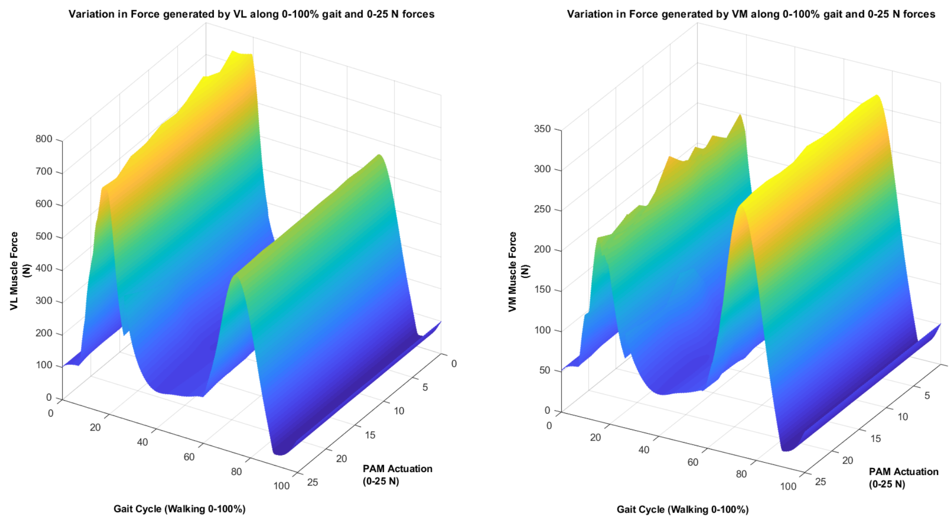

Figure C.7: Changes in force generated by VL and VM for PAM actuations 0-25 N

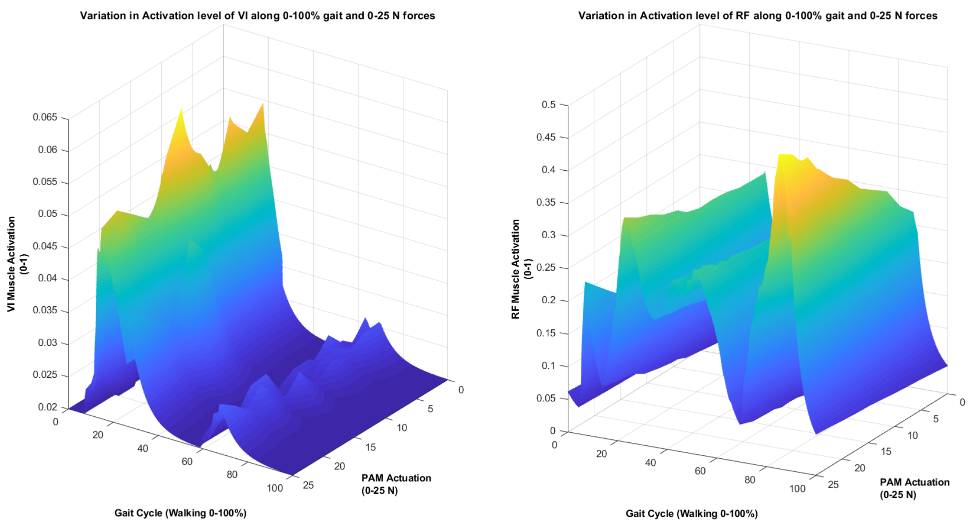

Figure C.8: Changes in muscle activation levels of VI and RF for PAM actuations 0-25 N

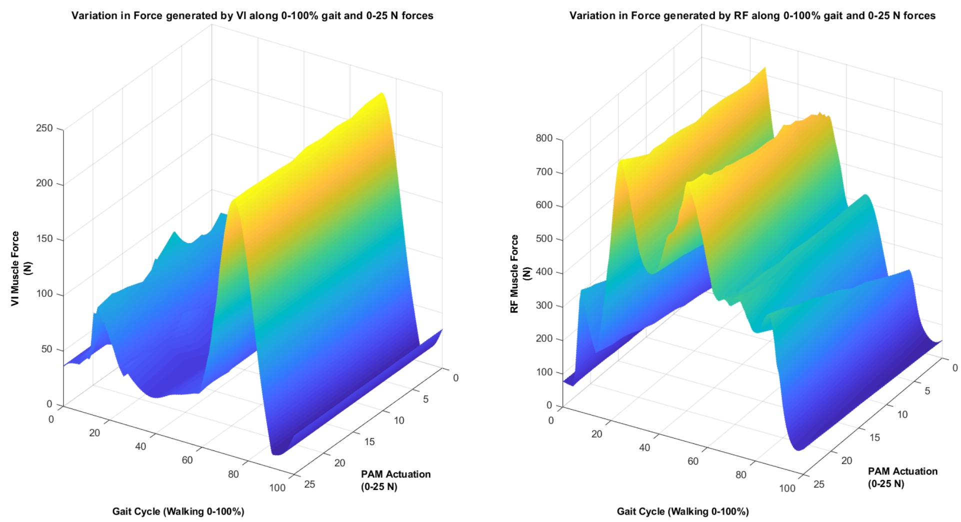

Figure C.9: Changes in force generated by VI and RF for PAM actuations 0-25 N

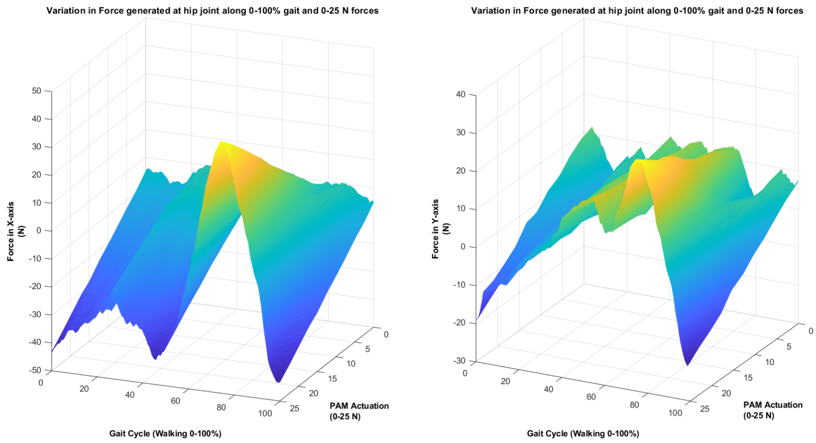

Figure C.10: Changes in Force generated at the hip joint in X-axis and Y-axis for PAM actuations 0-25 N

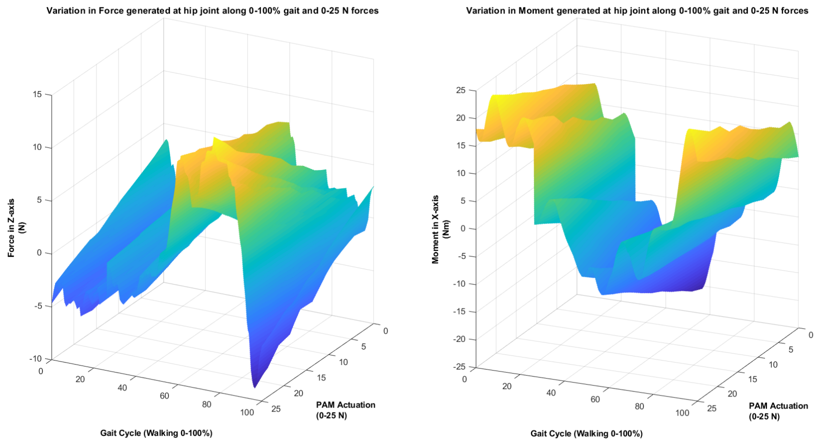

Figure C.11: Changes in Force and Moment generated at the hip joint in Z-axis and X-axis, respectively, for PAM actuations 0-25 N

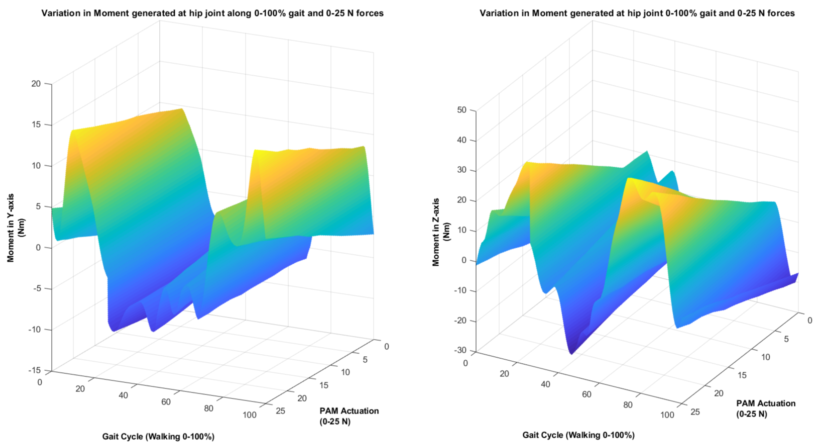

Figure C.12: Changes in Moment generated at the hip joint in Y-axis and Z-axis for PAM actuations 0-25 N

The pelvis joint connects the model to the reference ground frame while the ground reaction forces act as external forces to the calcaneus (heel bone). In the model the Force and Moment actuators are connected at the pelvis joint for providing the extra forces and moments required by the upper and the lower body for support. They behave like residual actuators for the whole body motion especially upper body. The optimal range of operation for force residual actuators is +10 to -10 N and for moment residual actuators it is -50 to 50 Nm. The above graphs, Fig. C.10, C.11 and C.12 shows the force in X-axis and Y-axis has crossed the optimal range with increasing PAM actuations. Similar case is seen in the moment of Z-axis. These variations could be because of the added weight of the PAM actuated brace. The motion of PAM actuators are focused on the mentioned axes in which the values have large variations with increasing PAM actuations but not in other axes.

Bibliography

Afonso, Morgana Pires (2015). "Modelling the gait of healthy and post-stroke individuals." In:

Ali, Azhar A. et al. (May 2017). "Combined measurement and modeling of specimen-specific knee mechanics for healthy and ACL-deficient conditions." en. In: *Journal of Biomechanics* 57, pp. 117–124. ISSN: 00219290. DOI: 10.1016/j.jbiomech.2017.04.008. URL: https://linkinghub.elsevier.com/retrieve/pii/S0021929017302075.

Battista et al., Nicolas (Mar. 2017). "IB2d: a Python and MATLAB implementation of the immersed boundary method." In: *Bioinspiration & Biomimetics* 12.3, p. 036003. DOI: 10.1088/1748-3190/aa5e08. URL: https://doi.org/10.1088/1748-3190/aa5e08.

Berchuck, Matthew (1990). "The effect of hamstring muscle compensation for anterior laxity in the ACL-deficient knee during gait." In: *Journal of Bone and Joint Surgery* 72.6, pp. 871–877.

Beynnon, Bruce D. et al. (2003). "The Effect of Anterior Cruciate Ligament Deficiency and Functional Bracing on Translation of the Tibia Relative to the Femur during Nonweightbearing and Weightbearing." In: *The American Journal of Sports Medicine* 31.1. PMID: 12531765, pp. 99–105. DOI: 10.1177/03635465030310012801. eprint: https://doi.org/10.1177/03635465030310012801. URL: https://doi.org/10.1177/03635465030310012801.

Bravo-Illanes, G et al. (July 2019). "IMU Sensor Fusion Algorithm for Monitoring Knee Kinematics in ACL Reconstructed Patients." en. In: *2019 41st Annual International Conference of the IEEE Engineering in Medicine and Biology Society (EMBC)*. Berlin, Germany: IEEE, pp. 5877–5881. ISBN: 978-1-5386-1311-5. DOI: 10.1109/EMBC.2019.8857431. URL: https://ieeexplore.ieee.org/document/8857431/.

Delp, S. L. et al. (1990). "An interactive graphics-based model of the lower extremity to study orthopaedic surgical procedures." In: *IEEE Transactions on Biomedical Engineering* 37.8, pp. 757–767. DOI: 10.1109/10.102791.

Durandau, Guillaume et al. (Dec. 2019). "Voluntary control of wearable robotic exoskeletons by patients with paresis via neuromechanical modeling." en. In: *Journal of NeuroEngineering and Rehabilitation* 16.1, p. 91. ISSN: 1743-0003. DOI: 10.1186/s12984-019-0559-z. URL: https://jneuroengrehab.biomedcentral.com/articles/10.1186/s12984-019-0559-z (visited on 01/25/2021).

Eguchi, R. et al. (2016). "Ground reaction force estimation using insole plantar pressure measurement system from single-leg standing." In: *2016 IEEE International Conference on Multisensor Fusion and Integration for Intelligent Systems (MFI)*, pp. 109–113. DOI: 10.1109/MFI.2016.7849475.

Esrafilian, A. et al. (Dec. 2020). "EMG-Assisted Muscle Force Driven Finite Element Model of the Knee Joint with Fibril-Reinforced Poroelastic Cartilages and Menisci." en. In: *Scientific Reports* 10.1, p. 3026. ISSN: 2045-2322. DOI: 10.1038/s41598-020-59602-2. URL: http://www.nature.com/articles/s41598-020-59602-2.

Ezati, Mahdokht (2019). "A review of simulation methods for human movement dynamics with emphasis on gait." en. In: p. 28.

Fleming, Braden C. et al. (Nov. 2000). "The Influence of Functional Knee Bracing on the Anterior Cruciate Ligament Strain Biomechanics in Weightbearing and Nonweightbearing Knees." en. In: *The American Journal of Sports Medicine* 28.6, pp. 815–824. ISSN: 0363-5465, 1552-3365. DOI: 10.1177/03635465000280060901. URL: http://journals.sagepub.com/doi/10.1177/03635465000280060901.

Fregly et al., Benjamin J (2012). "Personalized neuromusculoskeletal modeling to improve treatment of mobility impairments: a perspective from European research sites." en. In: *Journal of NeuroEngineering and Rehabilitation* 9.1, p. 18. ISSN: 1743-0003. DOI: 10.1186/

1743-0003-9-18. URL: http://jneuroengrehab.biomedcentral.com/articles/10.1186/1743-0003-9-18 (visited on 01/25/2021).

Horsman, M.D (2007). "The Twente lower extremity model: consistent dynamic simulation of the human locomotor apparatus." en. ISBN: 9789036526029 OCLC: 212421778. PhD thesis. S.l.: s.n.]

Hoy et al., Melissa G. (Jan. 1990). "A musculoskeletal model of the human lower extremity: The effect of muscle, tendon, and moment arm on the moment-angle relationship of musculotendon actuators at the hip, knee, and ankle." en. In: *Journal of Biomechanics* 23.2, pp. 157–169. ISSN: 00219290. DOI: 10.1016/0021-9290(90)90349-8. URL: https://linkinghub.elsevier.com/retrieve/pii/0021929090903498 (visited on 01/25/2021).

Kang, Bong-Soo et al. (May 2009). "Dynamic modeling of Mckibben pneumatic artificial muscles for antagonistic actuation." In: *2009 IEEE International Conference on Robotics and Automation*. 2009 IEEE International Conference on Robotics and Automation (ICRA). Kobe: IEEE, pp. 182–187. ISBN: 978-1-4244-2788-8. DOI: 10.1109/ROBOT.2009.5152280. URL: http://ieeexplore.ieee.org/document/5152280/.

Keizer, M. N. J. and E. Otten (Aug. 2019). "Passive anterior tibia translation in anterior cruciate ligament-injured, anterior cruciate ligament-reconstructed and healthy knees: a systematic review." In: *MUSCULOSKELETAL SURGERY* 103.2, pp. 121–130. ISSN: 2035-5106, 2035-5114. DOI: 10.1007/s12306-018-0572-6. URL: http://link.springer.com/10.1007/s12306-018-0572-6.

Khambati, Hussain M. (2019). *A soft robotic knee brace for improving knee stability in anterior cruciate ligament deficient patients*. Netherlands.

Lappas, Georgios (2020). *Estimation of liver respiratory motion using a surrogate signal based on a deep learning approach*. Netherlands.

Liu, Wen and Maitland (2000). "The effect of hamstring muscle compensation for anterior laxity in the ACL-deficient knee during gait." en. In: *Journal of Biomechanics*, p. 9.

Liu, Wen and Murray E. Maitland (2000). "The effect of hamstring muscle compensation for anterior laxity in the ACL-deficient knee during gait." In: *Journal of Biomechanics* 33.7, pp. 871–879. ISSN: 0021-9290. DOI: https://doi.org/10.1016/S0021-9290(00)00047-6. URL: http://www.sciencedirect.com/science/article/pii/S0021929000000476.

Lyu, Mingxing et al. (Aug. 2019). "Development of an EMG-Controlled Knee Exoskeleton to Assist Home Rehabilitation in a Game Context." en. In: *Frontiers in Neurorobotics* 13, p. 67. ISSN: 1662-5218. DOI: 10.3389/fnbot.2019.00067. URL: https://www.frontiersin.org/article/10.3389/fnbot.2019.00067/full.

Makhmalbaf, Hadi et al. (2013). "Accuracy of Lachman and Anterior Drawer Tests for Anterior Cruciate Ligament Injuries." en. In: . *NUMBER* 1.2, p. 4.

Marieswaran, M. et al. (Dec. 2018). "An extended OpenSim knee model for analysis of strains of connective tissues." In: *BioMedical Engineering OnLine* 17.1, p. 42. ISSN: 1475-925X. DOI: 10.1186/s12938-018-0474-8. URL: https://biomedical-engineering-online.biomedcentral.com/articles/10.1186/s12938-018-0474-8.

McLean et al., S. G. (Dec. 2003). "Development and Validation of a 3-D Model to Predict Knee Joint Loading During Dynamic Movement." en. In: *Journal of Biomechanical Engineering* 125.6, pp. 864–874. ISSN: 0148-0731, 1528-8951. DOI: 10.1115/1.1634282. URL: https://asmedigitalcollection.asme.org/biomechanical/article/125/6/864/459606/Development-and-Validation-of-a-3D-Model-to.

Millard, Matthew et al. (Feb. 1, 2013). "Flexing Computational Muscle: Modeling and Simulation of Musculotendon Dynamics." In: *Journal of Biomechanical Engineering* 135.2, p. 021005. ISSN: 0148-0731, 1528-8951. DOI: 10.1115/1.4023390. URL: https://asmedigitalcollection.asme.org/biomechanical/article/doi/10.

1115/1.4023390/371394/Flexing-Computational-Muscle-Modeling-and.

Naghibi, Hamid et al. (Mar. 2020). “A novel approach for optimal graft positioning and tensioning in anterior cruciate ligament reconstructive surgery based on the finite element modeling technique.” en. In: *The Knee* 27.2, pp. 384–396. ISSN: 09680160. DOI: 10.1016/j.knee.2020.01.010. URL: https://linkinghub.elsevier.com/retrieve/pii/S0968016020300090.

Naghibi Beidokhti, Hamid et al. (Oct. 2016). “A comparison between dynamic implicit and explicit finite element simulations of the native knee joint.” en. In: *Medical Engineering & Physics* 38.10, pp. 1123–1130. ISSN: 13504533. DOI: 10.1016/j.medengphy.2016.06.001. URL: https://linkinghub.elsevier.com/retrieve/pii/S1350453316301151.

Neumann, Donald (2010). *Kinesiology of the Musculoskeletal system*. en. Volve learning system v. 2. Elsevier. ISBN: 978-0-323-03989-5. URL: https://books.google.co.in/books?id=8ZhDPgAACAAJ.

Nicolella, Daniel P. et al. (Jan. 2011). “Dynamic Modeling of Knee Mechanics.” en. In: *Volume 2: Biomedical and Biotechnology Engineering; Nanoengineering for Medicine and Biology*. Denver, Colorado, USA: ASMEDC, pp. 517–523. ISBN: 978-0-7918-5488-4. DOI: 10.1115/IMECE2011-63940. URL: https://asmedigitalcollection.asme.org/IMECE/proceedings/IMECE2011/54884/517/354790.

Nikolopoulos, Filippos P. et al. (2020). “Personalized Knee Geometry Modeling Based on Multi-Atlas Segmentation and Mesh Refinement.” en. In: *IEEE Access* 8, pp. 56766–56781. ISSN: 2169-3536. DOI: 10.1109/ACCESS.2020.2982061. URL: https://ieeexplore.ieee.org/document/9042322/ (visited on 01/25/2021).

Odle, B. M. (2013). “Construction and assessment of a computer graphics-based model for wheelchair propulsion.” In:

Pamungkas, Daniel S et al. (Nov. 2019). “Overview: Types of Lower Limb Exoskeletons.” en. In: *Electronics* 8.11, p. 1283. ISSN: 2079-9292. DOI: 10.3390/electronics8111283. URL: https://www.mdpi.com/2079-9292/8/11/1283.

Parween, Rizuwana et al. (May 2019). “Methods for evaluating effects of unloader knee braces on joint health: a review.” en. In: *Biomedical Engineering Letters* 9.2, pp. 153–168. ISSN: 2093-9868, 2093-985X. DOI: 10.1007/s13534-019-00094-z. URL: http://link.springer.com/10.1007/s13534-019-00094-z.

Physiopedia (2016). *File:Structures of the knee.png — Physiopedia,* URL: https://www.physio-pedia.com/index.php?title=File:Structures_of_the_knee.png&oldid=144312.

Pizzolato, Claudio et al. (Nov. 2015). “CEINMS: A toolbox to investigate the influence of different neural control solutions on the prediction of muscle excitation and joint moments during dynamic motor tasks.” en. In: *Journal of Biomechanics* 48.14, pp. 3929–3936. ISSN: 00219290. DOI: 10.1016/j.jbiomech.2015.09.021. URL: https://linkinghub.elsevier.com/retrieve/pii/S0021929015005151 (visited on 01/25/2021).

Rajagopal, Apoorva et al. (Oct. 2016). “Full-Body Musculoskeletal Model for Muscle-Driven Simulation of Human Gait.” In: *IEEE Transactions on Biomedical Engineering* 63.10, pp. 2068–2079. ISSN: 0018-9294, 1558-2531. DOI: 10.1109/TBME.2016.2586891. URL: http://ieeexplore.ieee.org/document/7505900/.

Schlotman, Taylor Elyse (2017). “DYNAMIC SIMULATION AND ANALYSIS OF GAIT MODIFICATION FOR TREATING KNEE OSTEOARTHRITIS.” en. In: p. 128.

Schmitz, Anne and Davide Piovesan (Oct. 2016). “Development of an Open-Source, Discrete Element Knee Model.” en. In: *IEEE Transactions on Biomedical Engineering* 63.10, pp. 2056–2067. ISSN: 0018-9294, 1558-2531. DOI: 10.1109/TBME.2016.2585926. URL: http://ieeexplore.ieee.org/document/7501488/ (visited on 01/25/2021).

Seth, Ajay et al. (2011). "OpenSim: a musculoskeletal modeling and simulation framework for in silico investigations and exchange." en. In: *Procedia IUTAM* 2, pp. 212–232. ISSN: 22109838. DOI: 10.1016/j.piutam.2011.04.021. URL: https://linkinghub.elsevier.com/retrieve/pii/S2210983811000228.

Shelburne, Kevin B. and Marcus G. Pandy (Jan. 2002). "A Dynamic Model of the Knee and Lower Limb for Simulating Rising Movements." en. In: *Computer Methods in Biomechanics and Biomedical Engineering* 5.2, pp. 149–159. ISSN: 1025-5842, 1476-8259. DOI: 10.1080/10255840290010265. URL: http://www.tandfonline.com/doi/abs/10.1080/10255840290010265.

Shelburne et al., Kevin B. (Apr. 2005a). "Effect of Muscle Compensation on Knee Instability during ACL-Deficient Gait:" in: *Medicine & Science in Sports & Exercise* 37.4, pp. 642–648. ISSN: 0195-9131. DOI: 10.1249/01.MSS.0000158187.79100.48. URL: http://journals.lww.com/00005768-200504000-00017.

– (Nov. 2005b). "Muscle, Ligament, and Joint-Contact Forces at the Knee during Walking:" in: *Medicine & Science in Sports & Exercise* 37.11, pp. 1948–1956. ISSN: 0195-9131. DOI: 10.1249/01.mss.0000180404.86078.ff. URL: http://journals.lww.com/00005768-200511000-00018.

Sherman et al., Michael A. (2011). "Simbody: multibody dynamics for biomedical research." en. In: *Procedia IUTAM* 2, pp. 241–261. ISSN: 22109838. DOI: 10.1016/j.piutam.2011.04.023. URL: https://linkinghub.elsevier.com/retrieve/pii/S2210983811000241.

Solomon, Daniel H. et al. (Oct. 2001). "Does This Patient Have a Torn Meniscus or Ligament of the Knee?Value of the Physical Examination." In: *JAMA* 286.13, pp. 1610–1620. ISSN: 0098-7484. DOI: 10.1001/jama.286.13.1610. eprint: https://jamanetwork.com/journals/jama/articlepdf/194256/jrc00002.pdf. URL: https://doi.org/10.1001/jama.286.13.1610.

Solomonow, M. and M. Krogsgaard (Apr. 2001). "Sensorimotor control of knee stability. A review." en. In: *Scandinavian Journal of Medicine and Science in Sports* 11.2, pp. 64–80. ISSN: 0905-7188, 1600-0838. DOI: 10.1034/j.1600-0838.2001.011002064.x. URL: http://doi.wiley.com/10.1034/j.1600-0838.2001.011002064.x.

Stanev, D. et al. (2016). "ACL Reconstruction Decision Support: Personalized Simulation of the Lachman Test and Custom Activities." en. In: *Methods of Information in Medicine* 55.01, pp. 98–105. ISSN: 0026-1270, 2511-705X. DOI: 10.3414/ME14-02-0022. URL: http://www.thieme-connect.de/DOI/DOI?10.3414/ME14-02-0022 (visited on 01/26/2021).

Subit, Damien (2004). *A soft robotic knee brace for improving knee stability in anterior cruciate ligament deficient patients*. France.

Teufl, Wolfgang et al. (Feb. 2019). "Validity of inertial sensor based 3D joint kinematics of static and dynamic sport and physiotherapy specific movements." In: *PLOS ONE* 14.2, pp. 1–18. DOI: 10.1371/journal.pone.0213064. URL: https://doi.org/10.1371/journal.pone.0213064.

Thelen, Darryl G. (Feb. 2003). "Adjustment of Muscle Mechanics Model Parameters to Simulate Dynamic Contractions in Older Adults." In: *Journal of Biomechanical Engineering* 125.1, pp. 70–77. ISSN: 0148-0731. DOI: 10.1115/1.1531112. eprint: https://asmedigitalcollection.asme.org/biomechanical/article-pdf/125/1/70/5481649/70_1.pdf. URL: https://doi.org/10.1115/1.1531112.

Torry, Michael R. et al. (Dec. 2001). "Knee Stability Controlled by Hamstrings and Functional Knee Brace:" en. In: *JPO Journal of Prosthetics and Orthotics* 13.4, pp. 90–96. ISSN: 1040-8800. DOI: 10.1097/00008526-200112000-00008. URL: http://journals.lww.com/00008526-200112000-00008.

Trepczynski, Adam et al. (Dec. 2018). “Impact of antagonistic muscle co-contraction on in vivo knee contact forces.” en. In: *Journal of NeuroEngineering and Rehabilitation* 15.1, p. 101. ISSN: 1743-0003. DOI: 10.1186/s12984-018-0434-3. URL: https://jneuroengrehab.biomedcentral.com/articles/10.1186/s12984-018-0434-3.

Weinhandl, Joshua T. et al. (Aug. 2014). “Reduced hamstring strength increases anterior cruciate ligament loading during anticipated sidestep cutting.” In: *Clinical Biomechanics* 29.7, pp. 752–759. ISSN: 02680033. DOI: 10.1016/j.clinbiomech.2014.05.013. URL: https://linkinghub.elsevier.com/retrieve/pii/S0268003314001363.

Wesseling et al., Mariska (2018). “Objectifying Treatment Outcomes Using Musculoskeletal Modelling-Based Simulations of Motion.” en. In: *Handbook of Human Motion*. Ed. by Bertram Müller et al. Cham: Springer International Publishing, pp. 1–25. ISBN: 978-3-319-30808-1. DOI: 10.1007/978-3-319-30808-1_52-1. URL: http://link.springer.com/10.1007/978-3-319-30808-1_52-1 (visited on 01/25/2021).

Wikimedia (2008). *File:Diagramme$_g$enou.png$---Wikimedia$*,. URL: https://commons.wikimedia.org/wiki/File:Diagramme_genou.png#/media/File:Diagramme_genou.png.

Yamaguchi, Gary T. and Felix E. Zajac (Jan. 1989). “A planar model of the knee joint to characterize the knee extensor mechanism.” en. In: *Journal of Biomechanics* 22.1, pp. 1–10. ISSN: 00219290. DOI: 10.1016/0021-9290(89)90179-6. URL: https://linkinghub.elsevier.com/retrieve/pii/0021929089901796 (visited on 01/25/2021).

Zhang et al., Kuangeng (Mar. 2019). “Sensor Fusion for Predictive Control of Human-Prosthesis-Environment Dynamics in Assistive Walking: A Survey.” en. In: *arXiv:1903.07674 [cs]*. arXiv: 1903.07674. URL: http://arxiv.org/abs/1903.07674.